Hill-Robertson interference may bias the inference of fitness effects of new mutations in highly selfing species

Austin Daigle[1,2,3] and Parul Johri[1,2,4,*]

[1]Department of Biology, University of North Carolina, Chapel Hill, NC 27599

[2]Department of Genetics, University of North Carolina, Chapel Hill, NC 27599

[3]Curriculum in Bioinformatics and Computational Biology, University of North Carolina, Chapel Hill, NC 27599

[4]Integrative Program for Biological & Genome Sciences, University of North Carolina, Chapel Hill, NC 27599

*Correspondence can be addressed to these authors

Parul Johri

pjohri@unc.edu

Running title: Inferring fitness effects with selfing

Keywords: distribution of fitness effects, self-fertilization, Hill-Robertson interference, background selection, population structure

ABSTRACT

The accurate estimation of the distribution of fitness effects (DFE) of new mutations is critical for population genetic inference but remains a challenging task. While various methods have been developed for DFE inference using the site frequency spectrum of putatively neutral and selected sites, their applicability in species with diverse life history traits and complex demographic scenarios is not well understood. Selfing is common among eukaryotic species and can lead to decreased effective recombination rates, increasing the effects of selection at linked sites, including interference between selected alleles. We employ forward simulations to investigate the limitations of current DFE estimation approaches in the presence of selfing and other model violations, such as linkage, departures from semidominance, population structure, and uneven sampling. We find that distortions of the site frequency spectrum due to Hill-Robertson interference in highly selfing populations lead to mis-inference of the deleterious DFE of new mutations. Specifically, while accounting for the decrease in the effective population size due to linked effects of selection allows an accurate estimation of selection coefficients in moderately selfing populations, this correction is unable to accurately estimate selection coefficients in highly selfing populations when interference between selected alleles is pervasive. In addition, the presence of cryptic population structure with low rates of migration and uneven sampling across subpopulations leads to the false inference of a deleterious DFE skewed towards effectively neutral/mildly deleterious mutations. Finally, the proportion of adaptive substitutions estimated at high rates of selfing is substantially overestimated. Our observations apply broadly to species and genomic regions with little/no recombination and where interference might be pervasive.

INTRODUCTION

The distribution of fitness effects (DFE) of new mutations describes the continuum of selective effects of spontaneous mutations in a population and is critical for understanding the effects of natural selection on genetic variation (Eyre-Walker and Keightley 2007). Because of the considerable impact deleterious mutations can have on allele frequency patterns in a population, knowledge of the DFE is often necessary to produce accurate evolutionary models, which are required for unbiased estimates of both the demographic history of a population and the proportion of adaptive nucleotide substitutions in a lineage (Charlesworth 1994; Eyre-Walker and Keightley 2007; Bank *et al.* 2014; Johri *et al.* 2022a). While the DFE can be estimated with experimental approaches using random mutagenesis or mutation-accumulation lines (*e.g.*, Wloch *et al.* 2001; Estes *et al.* 2004; Sanjuán *et al.* 2004), it can also be inferred from the distribution of allele frequencies from population genetic data (Williamson *et al.* 2005; Eyre-Walker *et al.* 2006; Keightley and Eyre-Walker 2007; Galtier 2016). As many organisms cannot easily be cultured in laboratories, are not genetically manipulatable, and/or have large generation times, a population genetic approach remains an important and the only possible approach to estimating the DFE in some species.

Population genetic methods use putatively neutral sites to fit the demographic history or to account for other potential nuisance parameters, while selected sites are used to infer the DFE (by inferring the parameters of a prespecified probability distribution), conditional on the demographic history obtained from neutral sites (reviewed in Johri *et al.* 2022b). While most two-step population genetic approaches that infer the DFE make a series of assumptions, like random mating and the absence of effects of selection at linked sites, they appear to be robust to certain model violations like mutation rate variability (Tataru *et al.* 2017), linkage (Kim *et al.* 2017; Huang *et al.* 2021), population substructure (Kim *et al.* 2017), and some complex demographic changes (Kousathanas and Keightley 2013). This is because two-step inference methods are usually employed using interdigitated neutral and selected sites and might therefore correct for model violations that skew the neutral and selected SFS similarly. As an aside, because demographic history is unlikely to affect the SFS of neutral and very strongly deleterious mutations equally (Eyre-Walker *et al.* 2006), this might lead to slight inaccuracies in inference using methods that do not explicitly model population size changes. In fact, realistic simulations of chromosomal segments in both *Drosophila* (Huang *et al.* 2021) and humans

(Huber *et al.* 2017) suggest that inference of the DFE of new deleterious mutations remains accurate, despite the effects of background selection. Similarly, Kim *et al.* (2017) were able to accurately infer the parameters of the deleterious DFE in a simulated metapopulation that grew eight times larger and split into eight isolated populations. However, since migration was not simulated between these populations, the effects of population structure on DFE inference have not been fully explored.

Despite significant progress, not much work has been done on understanding the effects of non-random mating, in particular self-fertilization, on the inference of the DFE using population genetic approaches. Self-fertilization or selfing (*i.e.*, an individual mating with itself) is common across all eukaryotic species - about 35% of all seed plants and ~50% of all animals exhibit moderate to high rates (50-100%) of selfing (Goodwillie *et al.* 2005; Jarne and Auld 2006). It is thus important to thoroughly investigate if current methods can be used to obtain accurate parameters of the DFE in partially selfing organisms. A transition from random mating to partial selfing has several effects on the population. Firstly, the increase of nonrandom mating in a partially selfing population decreases the effective population size (N_e), due to a reduction in the amount of independently sampled gametes (Pollak 1987) . Note that while the amount of drift experienced by a mutation is larger with a higher rate of selfing, the mean change in allele frequency at a selected locus is also greater, due to the increased frequency of homozygotes (Charlesworth and Charlesworth 1987; Caballero and Hill 1992; Charlesworth 1992). There is no change in the probability of fixation of semidominant mutations, but the probability of fixation of recessive or partially recessive beneficial mutations is increased by selfing, and the probability of fixation of recessive or partially recessive deleterious mutations is slightly reduced (Caballero and Hill 1992; Charlesworth 1992). Thirdly, increased homozygosity in the genomes of partially selfing organisms results in a higher proportion of recombination events occurring on nearly identical chromosomes, which decreases the effective rate of recombination (Nordborg 2000). This effect increases the extent of background selection (BGS; Charlesworth *et al.* 1993; Charlesworth and Charlesworth 1998; Charlesworth 2003) and selective sweeps (Hedrick 1980; Hartfield and Bataillon 2020) experienced by the population. Finally, as the effective rate of recombination is lowered drastically in highly selfing populations, there can be a further decrease in the efficacy of selection due to Hill-Robertson interference (HRI) between selected loci (Hill

105 and Robertson 1966; McVean and Charlesworth 2000; Comeron and Kreitman 2002; Hartfield
106 and Glémin 2014, 2016).
107 Hill-Robertson interference (HRI) describes how the efficacy of selection at an allele at
108 one locus can be reduced due to the segregation of selected alleles at a second linked locus (Hill
109 and Robertson 1966; Felsenstein 1974). While BGS and selective sweeps are also a type of HRI,
110 those models assume that selection is strong and that there is no interference between selected
111 sites (reviewed in Charlesworth and Jensen 2021). However, because weakly selected mutations
112 can segregate in the population for longer times, interference between them can become
113 important especially if they are sufficiently prevalent (McVean and Charlesworth 2000;
114 Comeron and Kreitman 2002). Such interference between weakly selected alleles can result in
115 reduced efficacy of selection and has been termed as interference selection (Comeron *et al.* 1999;
116 Comeron and Kreitman 2002) or weak selection HRI (McVean and Charlesworth 2000; Kaiser
117 and Charlesworth 2009). Moreover, the effects of such interference have been shown to extend
118 to more strongly selected mutations in cases where recombination is greatly reduced (Kaiser and
119 Charlesworth 2009). We therefore refer to the effects of interference selection/weak selection
120 HRI as simply HRI in this study. Since the entire genomes of populations with high selfing rates
121 have greatly reduced effective recombination rates (Nordborg 2000) and deleterious mutations
122 are prevalent across the genome (Bank *et al.* 2014), HRI is likely to play an important role in
123 determining the dynamics of deleterious mutations in such populations.
124 Unlike the model of classical BGS, where deleterious alleles are at deterministic
125 mutation-selection equilibrium, selected sites in populations or genomic regions with pervasive
126 HRI depart from the standard equilibrium (Comeron and Kreitman 2002; Kaiser and
127 Charlesworth 2009; Seger *et al.* 2010; O'Fallon *et al.* 2010; Nicolaisen and Desai 2013). The site
128 frequency spectra (SFS) of neutral and selected sites affected by HRI are skewed towards rare
129 variants and become more similar to each other as the strength of HRI increases, and these
130 changes cannot be summarized as a simple change in effective population size (Comeron and
131 Kreitman 2002; Kaiser and Charlesworth 2009; Seger *et al.* 2010; O'Fallon *et al.* 2010;
132 Nicolaisen and Desai 2013; Good *et al.* 2014). More recent work assuming equal selection
133 coefficients across deleterious alleles has shown that when HRI is sufficiently common, the
134 nucleotide site diversity can be entirely described by the variation of fitness between individuals
135 in the population. However, populations with different combinations of average selection

136 coefficients, recombination, and mutation rates can have the same nucleotide diversity in this
137 regime (Good *et al.* 2014), suggesting difficulties in estimating a distribution of selection
138 coefficients along with other population genetic parameters in populations with little/no
139 recombination. While, a recent study suggested that the population-scaled fitness effects of
140 mutations are mis-inferred due to linked effects of selection when the probability of selfing is
141 sufficiently high (Gilbert *et al.* 2022), the role of HRI (specifically interference) remains unclear.
142 Here, we thoroughly characterize how HRI and other linked effects of selection might
143 bias the inference of both population-scaled as well as direct estimates of selection coefficients in
144 highly selfing species and in regions of low recombination for a variety of DFE shapes. To
145 investigate other potential causes of DFE mis-inference in partially selfing natural populations,
146 we explore the effects of changing the dominance coefficients, coding density, and number of
147 selected sites, as well as the effects of cryptic population structure and sampling on DFE
148 inference. Moreover, we characterize the accuracy of inference of both the DFE of new
149 deleterious mutations as well as the proportion of adaptive substitutions.
150
151
152 **METHODS**
153 **Simulations**
154 All simulations were performed using the forward simulator SLiM (version 4.0.1; Haller and
155 Messer 2023). The genome architecture and population parameters were modeled to mimic the
156 genomes of *C. elegans* populations because they have a high rate of selfing, which has been
157 estimated to be 98%-99.9% using laboratory observations (Hodgkin 1983; Anderson *et al.* 2010),
158 field work, and population genetic analyses (Barrière and Félix 2005, 2007). A chromosome with
159 an intron-exon structure was simulated such that each gene consisted of 6 exons (250 bp in
160 length) and 5 introns (100 bp in length). Genes were interspersed with intergenic regions of
161 length 3000 bp each. These numbers were close to the median of the length of exons, introns,
162 and intergenic regions observed in the *C. elegans* genome with a gene density of ~1 gene every
163 5kb (*C. elegans* Sequencing Consortium 1998). The *C. elegans* genome comprises 30% coding,
164 25% intronic, and 45% intergenic regions (*C. elegans* Sequencing Consortium 1998). In line
165 with these genome-wide characteristics, our simulated genome comprised of 30% coding, 10%
166 intronic, and 60% intergenic regions, and a total of 500 genes, resulting in a full chromosomal

167 length of 2,503,000 bp. All introns and intergenic regions were assumed to be neutral, while
168 exons experienced selection.
169 To take synonymous sites into account, 25% ($= f_{neu}$) of all mutations in exons were
170 assumed to be fully neutral (with s=0) while the rest were under selection. Of the selected
171 mutations, a fraction f_{pos} were assumed to be beneficial, where f_{pos} was assumed to be either
172 0.0, 0.01, or 0.001, and the rest ($1 - f_{pos} - f_{neu}$) were deleterious. The DFE of deleterious
173 mutations was assumed to be a gamma distribution, parametrized by the shape parameter (β) and
174 the mean population-scaled selection coefficient ($\gamma = 2N_e\overline{s_d}$), where $\overline{s_d}$ is the mean selective
175 disadvantage of the mutant homozygote relative to wildtype. Three different deleterious DFEs
176 were modeled, representing fitness effects skewed towards mildly, moderately, and strongly
177 deleterious classes respectively (Table 1). The DFE of beneficial mutations was assumed to be
178 exponential with mean $2N_e\overline{s_a} = 200$, where $\overline{s_a}$ is the mean selective advantage of the mutant
179 homozygote relative to wildtype. All mutations were assumed to be semidominant (where $h =$
180 0.5) unless otherwise specified.
181 A Wright-Fisher population under equilibrium was simulated with a population size (N_e)
182 of 500,000 diploid individuals (following Gilbert *et al.* 2022) and with varying probabilities of
183 selfing – 0%, 50%, 80%, 90%, 95%, and 99%, where $N_e = N$ for 0% selfing. Mutation (μ) and
184 recombination (r) rates were assumed to be constant at 3.3×10^{-9} per site/generation (Denver *et*
185 *al.* 2004; Konrad *et al.* 2019; Saxena *et al.* 2019) and 3.12×10^{-8} per site/generation (Rockman
186 and Kruglyak 2009), respectively. Simulations were conducted with a population size of 5000
187 diploid individuals, with a rescaling factor (Q) of 100, and rates of mutation and recombination
188 as well as selection coefficients were correspondingly adjusted so that the population-scaled
189 parameters $N\mu$, Nr, and Ns were equivalent to a population of 500,000. Simulations were run
190 for a total of $14N$ generations, where $10N$ generations corresponded to the burn-in period and
191 $4N$ generations were used to calculate the number of substitutions and where N represents the
192 scaled population size. Five replicates of each evolutionary scenario were simulated and the DFE
193 was estimated for each replicate separately.
194
195 *Single-locus simulations with selfing*: To investigate the effects of selfing on DFE inference
196 without linkage, selected, semidominant mutations were simulated at single sites with
197 probabilities of selfing of 0%, 50%, and 99%. The s_d of deleterious mutations were drawn from

198 the gamma distributions shown in Table 1. As allele frequencies of neutral mutations are
199 unaffected by linkage in the absence of selected mutations, 187,500 neutral sites were simulated,
200 which is equivalent to the number of neutral sites simulated in the simulations of 500 *C. elegans*
201 genes. 50,000 selected sites were simulated for each scenario (compared to 562,500 selected sites
202 in previous simulations), then paired with neutral mutations simulated with the appropriate
203 selfing rate. The simulations of individual selected sites and the neutral sites used rescaled values
204 of N, μ, and r equal to 5,000 individuals, 3.3×10^{-7} per site/generation and 3.12×10^{-6} per
205 site/generation respectively, which is equivalent to the previous simulations with linkage. All
206 simulations were run for $14N$ generations with $10N$ burn-in generations.
207
208 *Simulations under low recombination rates with no selfing*: To clarify if the lower effective
209 recombination rates in a partially selfing population were responsible for DFE mis-inference, we
210 conducted simulations with low recombination rates and 0% selfing. As before, these simulations
211 were conducted assuming a census size of 500,000 diploid individuals and rescaled by a factor of
212 100 to 5,000 individuals. The *C. elegans* recombination rate of 3.12×10^{-8} was thus rescaled to
213 3.12×10^{-6}, and multiplied by 0.5, 0.1, 0.05, 0.01, 0.005, or 0.001 to determine a final
214 simulated recombination rate. Beneficial mutations were not included in these simulations.
215
216 *Simulations with varying dominance coefficients*: All selected mutations shared a single
217 dominance coefficient of 0.1, 0.25, or 0.75. Populations with selfing probabilities of 0%, 50%,
218 and 99% were simulated and compared to the original simulations (where $h = 0.5$).
219
220 *Simulations under varying coding density and chromosome size*: Simulations were performed
221 with varying coding densities by varying the intergenic lengths - 1500 bp and 500 bp. The total
222 number of genes was not increased in these simulations. Thus, in the simulations with 1500 bp
223 intergenic regions, the simulated genome was comprised of ~43% coding, ~14% intronic, and
224 ~43% intergenic regions, with a total length of 1,752,100 bp. In the simulations with 500 bp
225 intergenic regions, the genome was comprised of ~55% coding, ~18% intronic, and ~27%
226 intergenic regions, with a total length of 1,376,650 bp. These simulations were run with
227 probabilities of selfing equal to 0%, 50%, and 99%.

To study the effects of a more realistically sized chromosome on DFE inference in selfers, simulations where the total number of genes was increased from 500 to 3000 were conducted, corresponding to approximately the number of genes observed on the first chromosome of the *C. elegans* genome. This increased the size of the simulated chromosome to 15,018,000 bp, which is close to the true size of *C. elegans* chromosome I (15,072,434 bp) (https://www.ncbi.nlm.nih.gov/datasets/genome/GCF_000002985.6/; last accessed in Dec. 2023).

Simulations with varying rescaling factors: To investigate the impact of rescaling of population sizes in our forward simulations, simulations were conducted with the rescaling factor $Q = 50$, 20, and 10, where the population-scaled parameters $N\mu$, Nr, and Ns were equivalent to a population of 500,000. Simulations were run for a total of $14N$ generations, where $10N$ generations corresponded to the burn-in period and $4N$ generations were used to calculate the number of substitutions and where N represents the scaled population size. Due to the excessive run time of unscaled simulations, simulations were only run for populations with selfing rates of 95% and 99%. For $Q = 10$, only one replicate of DFE3 at 95% selfing and three replicates each for DFE2 and DFE3 at 99% selfing reached completion.

Quantifying the effect of BGS in simulated data

To determine the theoretically expected neutral nucleotide diversity (π) in simulations with partial selfing, we calculated the expected effective population size after correcting for selfing (N_{self}) as $N_{self} = N/(1 + F)$, where $F = P_{self}/(2 - P_{self})$, and P_{self} represents the proportion of selfing individuals in a population per generation (Pollak 1987). Without the linked effects of selection, the neutral π is expected to be approximated by $\pi \sim \theta = 4N_{self}\mu$. In simulations with deleterious mutations, the extent of BGS was quantified as the observed nucleotide diversity (π_{obs}) at neutral sites relative to that expected under strict neutrality, *i.e.*,

$$B = \frac{\pi_{obs}}{4N_{self}\mu} \quad (1)$$

Simulations with population structure

To study the effects of population structure on DFE inference in selfers, a finite island model (Maruyama 1970) with five demes and an equal probability of exchange of migrants between all demes was considered. Note that in this model the migration rate is independent of the selfing rate, which applies well to animals but is not necessarily the case in plant species because selfing can prevent pollen dispersal (reviewed in Sicard and Lenhard 2011). Scenarios with different migration rates were simulated such that the effective metapopulation size remained constant and equivalent to the size of the panmictic population simulated above. Genome structure was identical to that in the previous simulations mimicking *C. elegans* genome architecture. In a metapopulation with d demes and a deme effective population size N_{deme}, the mean coalescence time for a pair of alleles sampled from the same deme (T_S) is given by the following equation (Nei 1973; Slatkin and Voelm 1991; Charlesworth and Charlesworth 2010):

$$T_S \sim 2dN_{deme} \tag{2}$$

The mean coalescence time for a pair of alleles sampled from different demes (T_B) is given by (Nei 1973; Slatkin and Voelm 1991; Charlesworth and Charlesworth 2010):

$$T_B \sim 2dN_{deme} + \frac{(d-1)}{2m} \tag{3}$$

where the migration rate m is the probability that an allele in one deme is derived by migration from any other deme in a generation (which means that the migration rate between any two demes is equal to $\frac{m}{d}$). Combining these two equations gives the mean coalescence time (T_T) for a pair of alleles drawn from the entire metapopulation (Nei 1973; Slatkin and Voelm 1991; Charlesworth and Charlesworth 2010):

$$T_T \sim 2dN_{deme} + \frac{(d-1)^2}{2dm} \tag{4}$$

To keep the effective size of the metapopulation ($0.5T_T$) equivalent to the rescaled size of 5,000 individuals used in previous simulations, N_{deme} and m were varied such that T_T remained equal to 10,000. To allow a wide range of migration rates, $N_{deme}m$ was varied from 10, 2, 1, 0.5, and 0.1 in populations with 0%, 50%, and 99% selfing, with separate simulations for DFE1, DFE2, and DFE3. The exact parameters used in each simulation can be found in Supplementary Table 7. Parameters were chosen so that the predicted F_{ST} of the entire metapopulation ($F_{ST} = \frac{T_T - T_S}{T_T}$) would cover a range of values (from 0.02 to 0.76) matching previously estimated values for *C. elegans* populations in the literature (from 0.15 to 0.43; Cutter 2006). Neutral simulations with identical genome structure and migration parameters were used to verify the joint effects of population structure and selfing on neutral nucleotide diversity and F_{ST}, and were found to yield expected results (Supplementary Table 8). The expected neutral nucleotide diversity for partially selfing populations was calculated assuming that the effective size of each deme will be equivalent to $N_{deme,self} = \frac{N_{deme}}{1+F}$, which was used to calculate the appropriate T_T and T_S values for each evolutionary scenario. In SLiM, m represents the proportion of individuals in a deme that are migrants each generation. Therefore, m still represents the probability that an allele is derived from migration each generation, and $N_{deme}m$ represents the number of diploid migrants per deme per generation.

Twenty genomes were sampled from each deme (totaling 100 genomes from the metapopulation) for DFE inference. To understand the effects of uneven sampling on DFE inference, two alternative sampling schemes were employed. In the first, 60 genomes were sampled from one deme, while 10 genomes were drawn from the remaining four demes. In the second, 35 genomes were drawn from two demes, while 10 genomes were drawn from the remaining three demes.

Calculating the SFS and the number of adaptive substitutions from simulations

The full output provided by SLiM was used to generate the site frequency spectra of neutral and selected mutations in exonic regions individually. The fixed class was obtained as the number of substitutions that occurred after the burn-in period ($= 10N$ generations). The zero class was calculated by subtracting the number of polymorphic and fixed sites from the total number of

317 sites for both neutral ($= 0.25 \times$ number of exonic sites) and selected ($= 0.75 \times$ number of
318 exonic sites) mutations respectively. Scripts to calculate the SFS are available at
319 https://github.com/JohriLab/DFESelfing/tree/main/calculateSFS.
320
321 The true fraction of beneficial substitutions (α) in simulations was obtained as follows:
322
323 $$\alpha = \frac{number\ of\ substitutions\ with\ 2N_e s_a > 5}{number\ of\ substitutions\ at\ selected\ sites} \quad (5)$$
324
325
326 Only substitutions that occurred after the burn-in with $2N_e s_a > 5$ were included when
327 calculating the true value of α in order to match the assumptions of GRAPES.
328
329 **DFE-alpha**
330 *Est_dfe* (Keightley and Eyre-Walker 2007) was employed to infer the DFE of deleterious
331 mutations. We fitted a two-epoch model, with starting values of $t2$ (time of change), β, and s_d
332 equal to 50, 0.5, and -0.01 respectively. $N2$ (current size) and $t2$ were also set to be variable. In
333 the absence of positive selection, the unfolded SFS was used as input, and the fold setting was
334 set to 0. In the presence of beneficial mutations, the folded SFS was used instead. DFE-alpha
335 provides the most likely estimate of the expected value of $\overline{s_d}$, the shape parameter (β) of the
336 gamma distribution, and a weighted effective population size (N_w). These parameters were used
337 to obtain the proportion of mutations (f_0, f_1, f_2, f_3) in the four classes- effectively neutral ($0 \leq$
338 $2N_w s_d < 1$), weakly deleterious ($1 \leq 2N_w s_d < 10$), moderately deleterious ($10 \leq 2N_w s_d <$
339 100), and strongly deleterious ($100 \leq 2N_w s_d$), respectively.
340
341 **GRAPES**
342 The program GRAPES (Eyre-Walker and Keightley 2009; Galtier 2016), Version 1.1.1
343 (https://github.com/BioPP/grapes/releases/tag/v1.1.1) was used to infer the full DFE using
344 simulations with and without positive selection. GRAPES provides the maximum likelihood
345 estimate of the shape parameter (β) and the expected population-scaled mean strength of
346 selection in terms of $2N_e\overline{s_d}$, in order to characterize the gamma distribution representing the

deleterious DFE. GRAPES also infers the parameters of the beneficial DFE, including the proportion of substitutions that are beneficial mutations (α) and the mean population-scaled strength of selection favoring new advantageous mutations $2N_e\bar{s_a}$, assuming that advantageous selection coefficients are exponentially distributed. The unfolded SFS was provided as input for both scenarios (with and without positive selection). In simulations without positive selection, the default parameters for the GammaZero model were used (*i.e.*, parameters of the beneficial DFE were not inferred). In the presence of positive selection, the estimated beneficial DFE was assumed to follow an exponential distribution (*i.e.*, the GammaExpo model was used), consistent with our simulations. As GRAPES can use either the folded or the unfolded SFS to provide estimates of the beneficial DFE, we performed inference using the unfolded and folded SFS separately to compare the results of both estimation methods. These parameters were accordingly used to obtain the values f_0, f_1, f_2, f_3, representing the classes of the deleterious DFE as described above.

Comparison of the expected and estimated DFE when mutations are semidominant

In a partially selfing population, diffusion theory provides the following mean ($M_{\Delta q}$) and variance ($V_{\Delta q}$) of the change in allele frequency (q) assuming that the change (Δq) in allele frequency is small (Caballero *et al.* 1991):

$$M_{\Delta q} = q(1-q)s[h + q(1-2h) + F(1-q-h+2qh)] \tag{6}$$

$$V_{\Delta q} = \frac{q(1-q)}{2N_{self}} = \frac{q(1-q)(1+F)}{2N} \tag{7}$$

For completely additive mutations ($h = 0.5$), the mean reduces to:

$$M_{\Delta q} = \frac{q(1-q)s(1+F)}{2} \tag{8}$$

In a panmictic population (of size N) with random mating, the mean and variance of change in allele frequency (assuming semidominance) is given by:

$$M_{\Delta q} = \frac{q(1-q)s}{2} \tag{9}$$

$$V_{\Delta q} = \frac{q(1-q)}{2N} \tag{10}$$

Thus, by comparing the above set of equations, a selfing population of size N experiences more genetic drift than a randomly mating population of the same size (Caballero and Hill 1992). However, the mean change in allele frequency in selfing populations is also larger, by the same factor, $(1+F)$, and thus the fixation probability of mutations remains the same in a selfing *vs*. a randomly mating population (Charlesworth and Charlesworth 1987; Caballero and Hill 1992; Charlesworth 1992). Thus, for the case of additive mutations and not taking selection at linked sites into account, the expected DFE would be determined by $2N_{self}s_d(1+F) = 2\frac{N}{(1+F)}s_d(1+F) = 2Ns_d$. To account for the relative decrease in population size due to BGS or selective sweeps, the simulated DFE was also adjusted and presented as $2NBs_d$, where B was calculated using equation 1.

In the case of the estimated DFE, because DFE-alpha only infers a relative increase or decrease in population size ($\frac{N_2}{N_1}$), these estimates of demographic parameters should not be affected by selfing rates (where the factor $1+F$ will cancel out). We thus present our inferred DFE as $2N_ws_d$.

Comparison of the expected and estimated DFE when mutations are not semidominant

When mutations were not additive, our expected DFE was parameterized by $2N_{self}s_dh_{self}$, where

$$N_{self} = \frac{N}{1+F} \tag{11}$$

and

$$h_{self} = h + q(1-2h) + F(1-q-h+2qh) \tag{12}$$

Assuming that $q << 1$, this equation simplifies to:

$$h_{self} \sim h + F(1-h) \tag{13}$$

Note that this approximation is less accurate when selection is weak ($2Ns_d \sim 1$) and thus might not be as accurate for the DFE comprising predominantly weakly deleterious mutations. The estimated DFE (using DFE-alpha and GRAPES) was parameterized by $2N_w s_d h$ where $h = 0.5$ is assumed by both the programs.

Calculation of summary statistics from simulated data

In order to quantify the effects of HRI, the skew in the SFS towards rare alleles was measured using the summary statistic $\Delta\theta_w = 1 - (\frac{\pi}{\theta_w})$, which has been demonstrated to be less sensitive than Tajima's *D* to the number of SNPs used in the calculation (Becher *et al.* 2020). Here, π is the nucleotide diversity (Nei and Tajima 1981) and θ_w denotes Watterson's θ (Watterson 1975). Both summary statistics were calculated in nonoverlapping 5000 bp windows using *pylibseq* v. 0.2.3 (Thornton 2003). To summarize linkage disequilibrium, D' was calculated for pairs of polymorphisms at frequencies between 1% and 5% in each window. Only low-frequency SNPs were used for D' calculations to correct for the allele frequency dependence of linkage disequilibrium statistics (Lewontin 1988). Here D and D' Lewontin (1964) were computed by *pylibseq* as follows:

$$D = p_{AB} - p_A p_B \tag{14}$$

and

$$D' = \frac{D}{D_{max}} \quad (15)$$

where

if $D > 0$

$$D_{max} = \min(p_A p_b, p_a p_B) \quad (16)$$

if $D < 0$

$$D_{max} = \min(p_A p_B, p_a p_b) \quad (17)$$

where p_A and p_B represent the minor allele frequency for each polymorphism, p_a and p_b represent the major allele frequency, and p_{AB} represents the frequency of the haplotype AB. All summary statistics were calculated separately for neutral and selected polymorphisms in exonic regions.

RESULTS

Inference of the DFE of new deleterious mutations in self-fertilizing populations

We simulated a single *C. elegans*-like population with varying rates of selfing – 0, 50, 80, 90, 95, and 99% and three different DFEs (following a gamma distribution; parameters specified in Table 1) skewed towards mildly (DFE1), moderately (DFE2), and strongly deleterious (DFE3) classes respectively. Here we assumed that all new mutations were semidominant. We used DFE-alpha and GRAPES to infer the shape of the deleterious DFE, specified to be gamma-distributed. As expected, when there is no selfing, inference was accurate (Figure1, Supplementary Figure 1, Supplementary Table 1, Supplementary Table 2). As the selfing rate increased ($\geq 90\%$), the estimated DFE was skewed strongly towards the class of mildly deleterious mutations (Figure 1), when compared to the simulated DFE, with a particularly strong skew in the most highly selfing population, consistent with Gilbert *et al.* (2022). This mis-inference corresponded with large decreases in the mean values of population-scaled selection coefficients of the inferred gamma distributions (Supplementary Figure 1). The β parameter of the gamma distribution was also mis-inferred as the selfing rate increased, with the inferred β becoming 2-3× smaller than the simulated value at 99% selfing (Supplementary Table 2). While

465 the overall shape and skew of the DFE were largely recovered when there was some chance of
466 outcrossing (*e.g.*, with $P_{self} \sim 90\%$; Figure 1), the mean population-scaled selection coefficients
467 remained slightly biased even when selfing rates were as low as 80% (*e.g.* for DFE2;
468 Supplementary Figure 1, Supplementary Table 2).
469 Because BGS will lead to a decrease in the effective population size, we hypothesized
470 that the true population-scaled selection coefficients in our simulated populations are likely to be
471 smaller than those simulated (*i.e.*, $2Ns_d$). To account for the reduction in the efficacy of
472 purifying selection due to BGS, we corrected the simulated DFE with the relative rate of
473 coalescence (B) with and without BGS observed in the simulated population. Note that this
474 adjusted DFE accounts for the relative decrease in population size due to linked effects of
475 selection only, not due to selfing (see details in Methods). While the inferred DFE matches the
476 corrected expected DFE substantially well for moderate levels of selfing (Figure 1), the DFE
477 accounting for BGS is somewhat inaccurate at high selfing levels, especially for the DFEs with
478 more weakly and moderately deleterious mutations. That is, the inferred DFE tends to have both
479 more strongly deleterious mutations and nearly neutral mutations than the DFE accounting for
480 linked effects of selection and will thus result in the inference of a distribution of "*s*" that is more
481 platykurtic than the simulated distribution (Supplementary Figure 2). This suggests that a simple
482 rescaling of the effective population size can correct for the misinference when selfing rates are
483 low/moderate (when the population is likely experiencing classical BGS) but not when rates are
484 high (when the population is likely in the interference selection regime). As expected, this effect
485 is especially strong when the DFE consists of many weakly and strongly moderately mutations
486 (Supplementary Figure 2). We, therefore, conclude that Hill-Robertson interference (HRI)
487 among deleterious alleles is likely causing the mis-inference of the DFE of new mutations in
488 highly selfing populations.
489
490 As expected, the simulated DFEs were accurately estimated from single-locus simulations with
491 no linkage even in highly selfing populations (Supplementary Figure 3), despite a significant
492 reduction in the total number of segregating sites at high selfing (Supplementary Table 3).
493 Concordantly, the observed SFSs at selected and neutral sites were highly similar across different
494 selfing levels, confirming that selfing does not drastically influence the proportions of allele
495 frequencies in a population without linkage (Supplementary Figure 4), assuming that deleterious

496 mutations are additive. Importantly, as high rates of selfing increase the levels of homozygosity,
497 the site frequency spectrum (SFS) obtained from a random sample of diploid *individuals*
498 deviated starkly from one obtained by a random sampling of *genomes* (an example shown in
499 Supplementary Figure 5A). The inferred DFEs were very similar when we sampled individuals
500 *vs*. genomes (Supplementary Figure 5B) and thus all results that follow were obtained by
501 sampling genomes.
502
503
504 **The effects of linkage on DFE inference in regions of low recombination**
505 HRI is more likely in genomic regions of low recombination and may similarly bias DFE
506 inference. With decreasing rates of recombination (0.5, 0.1, 0.05, 0.01, 0.005, and 0.001×), the
507 extent of mis-inference of the DFE increased (Figure 2). As before, the estimated DFE was
508 strongly skewed towards mildly deleterious mutations compared to the simulated DFE,
509 consistent with a decrease in the efficacy of selection due to linked effects of selection.
510 The relative decrease in nucleotide diversity ($B = \frac{\pi}{\pi_0}$) due to background selection,
511 measured in simulations of regions with low recombination ($B \sim 0.05 - 0.92$) captures the range
512 of B values measured in the simulations with selfing and linkage ($B \sim 0.08 - 0.95$). To account
513 for the decrease in the effective population size due to BGS, the inferred DFE was compared to
514 the DFE given by the distribution of $2NBs_d$. Again, while the DFE accounting for BGS
515 explained the estimated DFEs quite well for higher recombination regions, at very low
516 recombination rates, it did not match the inferred DFEs. As with high selfing, the estimated
517 distribution of selection coefficients at low recombination was observed to be more platykurtic
518 than the DFE accounting for BGS, and mis-inference was much stronger at the lowest
519 recombination rates, even for the most strongly deleterious DFE (Supplementary Figure 6). This
520 reflects the fact that a simple rescaling effect of BGS (*i.e.*, the decrease in the rate of
521 coalescence) is unlikely to explain mis-inference observed in regions of very low recombination.
522 When recombination rates are extremely low, the probability of interference between selected
523 alleles at multiple loci increases, leading to a departure of the SFS from equilibrium. Overall,
524 increased HRI caused by severely reduced recombination rates, which are of particular
525 importance in selfing organisms, might lead to the observed DFE mis-inference.
526

527 **The quantification of HRI using summary statistics**

528 Much theoretical and computational work on HRI has suggested that the decrease in the efficacy
529 of selection results in a decrease in the nucleotide diversity at selected and linked neutral sites as
530 well as an increase in divergence at selected sites due to the increased fixation of deleterious
531 mutations (Comeron *et al.* 1999; McVean and Charlesworth 2000). Moreover, the site frequency
532 spectrum for selected and neutral sites is expected to be skewed towards low-frequency variants
533 as the strength of BGS and HRI increases (mimicking the genealogy of an expanding population;
534 Zeng and Charlesworth 2011; Walczak *et al.* 2012; Nicolaisen and Desai 2013; Good *et al.*
535 2014), and the nucleotide diversity and site frequency spectrum of selected mutations are
536 expected to become more similar to those of neutral mutations (Comeron and Kreitman 2002;
537 Kaiser and Charlesworth 2009; Seger *et al.* 2010; O'Fallon *et al.* 2010; Nicolaisen and Desai
538 2013). Because interference results in a gene genealogy with longer external branches than
539 expected under a standard neutral coalescent (Walczak *et al.* 2012; Nicolaisen and Desai 2013),
540 and consistent with a skew towards low-frequency alleles, new mutations are more likely to
541 occur on separate branches of the genealogy, generating negative LD. Thus signed measures of
542 linkage disequilibrium between selected mutations and nearby neutral sequences become more
543 negative as HRI becomes stronger (Hill and Robertson 1966; McVean and Charlesworth 2000;
544 Comeron and Kreitman 2002; Garcia and Lohmueller 2021). In addition, in populations with
545 pervasive HRI, the SFS has been observed to show non-monotonic behavior at high frequencies,
546 resulting in a U-shape, which deviates from the predictions of the classical BGS theory (Seger *et*
547 *al.* 2010; Neher and Hallatschek 2013; Good *et al.* 2014; Zeng and Corcoran 2015; Cvijović *et*
548 *al.* 2018).

549 In our simulations, the SFSs of neutral and selected sites shifted towards lower frequency
550 mutations and became more similar at 90% selfing and above (Figure 3A, Supplementary
551 Figures 7A & 8A), which is consistent with the extent of DFE mis-inference and with previously
552 simulated results in highly selfing populations (Charlesworth *et al.* 1993). In addition, the SFS at
553 high frequency alleles showed non-monotonic (U-shaped) behavior (Figure 3B, Supplementary
554 Figures 7B & 8B), which has been previously observed in populations with pervasive HRI
555 (Seger *et al.* 2010; Neher and Hallatschek 2013; Good *et al.* 2014) or very strong background
556 selection (Cvijović *et al.* 2018). Note that the SFS of neutral sites at 0% selfing was very similar
557 to the unlinked neutral SFS (Supplementary Figure 4), consistent with high *B* values. Trends in

558 $\Delta\theta_w$, a measure of the skewness of the SFS (with positive values indicating a relative increase in
559 rare alleles), were concordant with the patterns in the SFSs, with $\Delta\theta_w$ values for neutral and
560 selected sites sharply increasing and converging towards each other at 90% selfing and above
561 (Figure 4A). Values of $\Delta\theta_w$ at neutral sites nearly converge with values at selected sites at 99%
562 selfing, reflecting the reduced efficacy of selection and almost complete linkage.
563 For selfing rates between 80% and 95%, D' tended to become closer to 0 at both selected
564 and neutral sites (Figure 4B). This is similar to an effect observed in simulations by Kamran-
565 Disfani and Agarwal (2014), where partially selfing populations with intermediate selfing rates
566 showed increases in linkage disequilibria. This phenomenon is expected at higher selfing levels
567 if the efficacy of selection is not overwhelmed by HRI, because of correlations in homozygosity
568 at different loci across the genome (Roze and Lenormand 2005). At 99% selfing, D' values
569 became considerably more negative for selected and neutral sites, consistent with a population
570 experiencing pervasive HRI.
571
572 **Simulation rescaling alters the effects of HRI**
573 Due to computational time constraints, it was necessary to rescale the parameters $N\mu$, Nr, and
574 Ns for most simulations in this study by lowering N and increasing μ, r, and s by the rescaling
575 factor $Q = 100$. While equivalent equilibria are expected according to diffusion theory if the
576 population-scaled parameters are held constant (Hill and Robertson 1966; Crow and Kimura, M.
577 1970; Ewens 1979; Li 1987), it has previously been observed that high levels of rescaling can
578 increase the effects of HRI (Comeron and Kreitman 2002). To understand the effects of rescaling
579 at high selfing rates, we once again simulated *C. elegans*-like populations with 500 genes and
580 selfing rates of 95% and 99% and the three deleterious DFEs, with $Q = 50$, 20, and 10, though
581 at $Q = 10$ only a limited number of simulations were able to be completed within a reasonable
582 timeframe. We find that as Q decreases from the original value of 100, the effects of background
583 selection and HRI decrease, with the B values decreasing in a linear fashion with Q
584 (Supplementary Figure 9). While the extent of DFE mis-inference decreases as Q is lowered, it is
585 important to note that the DFEs estimated at low Q values and 99% selfing were still mis-
586 inferred, especially the DFEs with more weakly and moderately deleterious mutations. As
587 expected based on the inferred DFEs, the SFS at higher selfing rates and low Q was still skewed
588 towards lower frequency mutations and U-shaped, though less than at high Q (Supplementary

589 Figures 10-11). Thus, it is likely that fully unscaled simulations ($Q = 1$) would have even less
590 HRI effects, especially for the strongly deleterious DFE, though it is not unrealistic to expect
591 strong BGS and some interference between selected mutations based on the trends observed
592 here. For instance, we observed much stronger effects of BGS and substantially more mis-
593 inference of the DFE when larger genomic regions were simulated (Supplementary Figure 12),
594 suggesting full length chromosomes simulated at $Q = 1$ will likely have more pervasive linked
595 effects of selection. Indeed, Gilbert *et al.* (2022) conducted unscaled simulations of the entire
596 genome, including all full-length chromosomes and a reduced recombination rate in chromosome
597 centers, with *C. elegans*-like parameters and found a strong skew in their inferred DFEs relative
598 to their simulated DFEs at intermediate levels of selfing (see figure 4 of Gilbert *et al.*), so
599 exploration of our scaled simulations with pervasive HRI is still relevant to highly selfing
600 populations.
601
602 **Extent of mis-inference does not depend on coding density**
603 The effects of HRI are expected to increase when there is a higher density of selected sites, as
604 deleterious mutations arising in the population will be more closely linked on average (Comeron
605 and Kreitman 2002). Gene density varies along the *C. elegans* chromosomes, with higher gene
606 densities found in the chromosome centers than in the chromosome arms (*C. elegans* Sequencing
607 Consortium 1998). To understand if increases in coding density change the extent of DFE mis-
608 inference, we decreased the length of intergenic regions in our simulations, while keeping the
609 number and length of genes constant, producing simulations with coding densities 2× and 6×
610 higher than our original coding density. We observed no obvious changes in DFE inference in
611 these scenarios (Supplementary Figure 13), suggesting that DFE mis-inference will not increase
612 in more coding-dense regions of the genome, although local gene densities could increase more
613 than we simulated. In addition, the rate of recombination in *C. elegans* is higher in the gene-poor
614 chromosome arms than in the gene-rich cores (Rockman and Kruglyak 2009), which could
615 worsen DFE mis-inference in regions with high gene density due to low recombination rates.
616
617 **The impact of dominance on DFE inference**
618 DFE-alpha and GRAPES assume that all new mutations are semidominant, but it is known that
619 dominance coefficients of new deleterious mutations vary considerably and are partially

620 recessive on average, with strongly deleterious mutations tending to be highly recessive
621 (Simmons and Crow 1977; Agrawal and Whitlock 2011; Manna *et al.* 2011). The effect of
622 dominance on DFE inference is not fully understood. Most DFE inference methods assume that
623 new mutations are semidominant and thus provide estimates of the joint distribution of the
624 selection and dominance coefficients, "$s_d h$". A recent study by Wade *et al.* (2023) suggests that,
625 if there are recessive lethal mutations, current DFE inference approaches can lead to
626 underestimating the true proportion of strongly deleterious mutations, as more strongly
627 deleterious mutations are likely to persist in the population if they are recessive. Furthermore,
628 since selfing increases the levels of homozygosity in the genome, the efficacy of selection
629 against large effect and highly recessive deleterious mutations is expected to be greater
630 (Charlesworth and Charlesworth 1998), leading to more efficient purging of deleterious
631 mutations. Thus, with higher rates of selfing one might instead expect to observe a decrease in
632 the allele frequencies of mildly and moderately deleterious mutations, leading to the false
633 inference of the presence of more strongly deleterious mutations in the population.
634 To investigate the joint effects of dominance and selfing on DFE inference, we performed
635 simulations where all selected mutations had fixed dominance coefficients equal to 0.1, 0.25, or
636 0.75. Note that the outputs of DFE-alpha and GRAPES were adjusted to represent $2N_{self}s_d h_{self}$
637 rather than $2Ns_d$, and the expected values from the simulations were adjusted to account for the
638 dominance and homozygosity of selfing genomes (Caballero and Hill 1992), as described in
639 Methods. At 0% selfing, as new deleterious mutations became more recessive (especially when
640 $h = 0.1$), the distribution of the product of the selection and dominance coefficients was
641 somewhat mis-inferred. When mutations were predominantly moderately and strongly
642 deleterious, there was an underestimation of the proportion of strongly deleterious mutations
643 (Figure 5, Supplementary Table 5), consistent with Wade *et al.* (2023). Additionally, the
644 frequency of the nearly neutral class of mutations was underestimated in all three DFEs, an effect
645 that can also be observed to a smaller degree in Wade *et al.* (2023). However, when new
646 mutations were comprised largely of mildly deleterious mutations (*i.e.*, DFE1), there was an
647 overestimation of the fraction of strongly deleterious mutations. In contrast, when more
648 dominant mutations were simulated, DFE inference resulted in mis-inference towards both
649 weakly and strongly deleterious mutations, though this effect was fairly small. As expected, mis-

650 inference was stronger when the true DFE was skewed towards mildly deleterious mutations, as
651 these mutations are more likely to be present as homozygotes in the population.
652 As selfing increases homozygosity, the inferred DFEs in partially selfing populations at
653 different dominance levels are expected to become more similar to each other, making the
654 dominance of mutations a less important factor for the efficacy of selection (Caballero and Hill
655 1992; Charlesworth 1992). As expected, at 50% selfing, the DFE was inferred more accurately
656 (Supplementary Figure 14, Supplementary Table 5). While the dominance coefficient played a
657 negligible role in DFE inference when the selfing rate was 99%, the estimated DFEs were
658 strongly skewed towards mildly deleterious mutations (Figure 5). Thus, just as expected, at high
659 rates of selfing, dominance coefficients play a relatively minor role, while HRI and BGS are
660 primarily responsible for DFE mis-inference.
661 Increased purging of recessive deleterious mutations has been hypothesized to reduce
662 their average allele frequencies, leading to DFE mis-inference (Arunkumar *et al.* 2015; Gilbert *et*
663 *al.* 2022). However, observable effects of purging are likely to occur only when mutations are
664 highly recessive (Nei 1968) and strongly deleterious (Glémin 2003). Concordantly, we observed
665 that the distribution of allele frequencies of partially recessive ($h = 0.25$) mutations at
666 intermediate selfing levels was the same as those of semidominant mutations, suggesting that
667 increased purging of recessive deleterious alleles did not have a strong effect on the average
668 allele frequencies in a population sample at equilibrium (see the SFS in Supplementary Figure
669 15).
670
671 **Inference of the full DFE of new deleterious and beneficial mutations**
672 Both BGS and HRI lead to a decrease in the efficacy of selection at linked selected sites, thus
673 reducing the probability of fixation of beneficial mutations while increasing the probability of
674 fixation of deleterious mutations (Charlesworth 1992; Kamran-Disfani and Agrawal 2014). It is
675 therefore likely that the proportion of fixed mutations at selected sites that are beneficial (α) is
676 mis-estimated when effective recombination rates are low. We conducted simulations with 0%,
677 50%, 80%, 90%, 95%, and 99% selfing, where 0.1% and 1% of new mutations in exons were
678 beneficial, following an exponential distribution with $2N\bar{s_a} = 200$. When 0.1% of new exonic
679 mutations were beneficial, the inference of the deleterious DFE by GRAPES was fairly accurate
680 at 0% and 50% selfing (Figure 6A). However, the deleterious DFE was mis-inferred at a much

681 lower selfing rate than in scenarios without beneficial mutations and mis-inference was
682 particularly strong when the deleterious DFE was highly skewed towards weakly deleterious
683 mutations. When 1% of new mutations were beneficial, the deleterious DFE estimated by
684 GRAPES was strongly skewed towards nearly neutral mutations even at 0% selfing for the
685 weakly deleterious and moderately deleterious DFEs (Supplementary Figure 16). Due to
686 recurrent selective sweeps in this scenario as well as BGS, there is likely to be a substantial
687 decrease in effective population size experienced by selected alleles (and thus a reduced $2N_e s_d$).
688 We thus accounted for this decrease again by comparing the inferred DFE to the distribution of
689 $2N(\pi/\pi_0)s_d$, where π/π_0 represents the neutral nucleotide site diversity with and without
690 selection. Again, the DFE accounting for the decrease in the effective size did not explain the
691 inferred DFE at high selfing rates, including 95% selfing, suggesting that HRI effects might be
692 responsible for the mis-inference, even at moderate levels of selfing (Figure 6A). The selected
693 SFSs resembled the neutral SFSs in simulations with DFE mis-inference, reflecting the observed
694 results of DFE inference (Supplementary Figure 17). With a high rate of beneficial mutations
695 entering the population, hitchhiking can reduce the efficacy of selection on weakly deleterious
696 alleles (Campos and Charlesworth 2019), leading to the mis-inference of the DFE for the more
697 weakly deleterious DFEs. In addition, the failure of DFE inference programs to fully correct for
698 the presence of mildly beneficial alleles in the SFS could also have contributed to the observed
699 mis-inference (Tataru *et al.* 2017).
700 As the folded SFS might provide better estimates of the deleterious DFE when beneficial
701 mutations are segregating at high frequencies (Keightley and Eyre-Walker 2007; Eyre-Walker
702 and Keightley 2009), we also tested the inference using the folded SFS. Overall, the deleterious
703 DFE inferred by GRAPES was comparable to the unfolded results when the folded SFS was
704 used (Supplementary Figures 18A & 19A). However, the DFEs estimated by DFE-alpha were
705 biased towards weakly deleterious mutations even with no selfing, with much larger uncertainty
706 in the estimated DFE at high selfing levels, especially when 1% of all new selected mutations
707 were beneficial. This indicates that folding the SFS is inadequate to correct for the mis-inference
708 of the deleterious DFE when the rate of new beneficial mutations is extremely high.
709 As expected, the true fraction of beneficial substitutions (α) decreased as the selfing rate
710 increased (Figure 6B, Supplementary Figure 16B). Changes in this parameter were driven by
711 both increases in the number of deleterious substitutions ($\sim 2-4\times$ higher at 99% selfing

712 relative to 0% selfing) as well as the decreases in the number of beneficial substitutions (~3 ×
713 lower at 99% selfing relative to 0% selfing; Supplementary Table 6), consistent with previous
714 observations in Kamran-Disfani and Agrawal (2014). In simulations with both 0.1% beneficial
715 mutations and 1% beneficial mutations, α tended to be overestimated for the weakly deleterious
716 DFE at all selfing levels, with mis-inference increasing steadily as the selfing rate increased. For
717 the moderately and strongly deleterious DFEs, α was only overestimated at high selfing levels,
718 with the strongly deleterious DFE corresponding with the most accurate inference of α. This is
719 consistent with the expectation that a decrease in the efficacy of selection will increase the
720 fixation of weakly deleterious alleles, which will be misinterpreted as beneficial fixations by
721 GRAPES, leading to an overestimation of α at high selfing levels. Very similar trends were
722 observed when the folded SFS was used to estimate α (Supplementary Figures 18B & 19B).
723 Overall, at high selfing levels, α values were substantially overestimated by GRAPES.
724
725 **Effects of population structure and sampling on the accuracy of inference**
726 A final factor that could bias DFE inference in partially selfing populations is population
727 structure because the inference procedure of DFE-alpha and GRAPES is not designed to account
728 for the effects of population structure on the SFS. Moreover, selfing populations tend to have
729 highly structured populations, and DFE inference in the context of population structure has been
730 largely unexplored, though the effects of cryptic structure (without migration) were tested in Kim
731 *et al.* (2017). Here, we simulated an island model, with five demes that exchanged migrants at a
732 total rate m each generation. Multiple values of m were used to vary the degree of isolation
733 between demes in this model, and the number of individuals in each deme (N_{deme}) was varied so
734 that the effective size of the metapopulation (N_{meta}) was equivalent to 500,000 individuals
735 (Supplementary Table 7). Under strict neutrality and while selfing was taken into account (see
736 Methods), the neutral nucleotide diversity of the entire metapopulation ($2T_T\mu$), of individual
737 subpopulations ($2T_S\mu$), and F_{ST} was equal to theoretical expectations (equations 2-4,
738 Supplementary Table 8). We performed simulations at $N_{deme}m = 0.1,\ 0.5,\ 1,$ and 2, which
739 corresponded to $F_{ST} = 0.76,\ 0.38,\ 0.24,$ and 0.14 respectively at 99% selfing. These values
740 were chosen to mimic F_{ST} values observed empirically amongst *C. elegans* populations, which
741 range from 0.44 to 0.83 (Barrière and Félix 2005; Richaud *et al.* 2018).

742 Population structure by itself did not result in mis-inference of the DFE when the rate of
743 migration was sufficiently high (*i.e.*, $N_{deme}m = 2, 1,$ and 0.5). High selfing rates with
744 population structure again led to inferring a DFE skewed almost entirely towards mildly
745 deleterious mutations, thus producing a very similar extent of mis-inference as that observed in a
746 panmictic population (Supplementary Figure 20 A, B, and C, respectively). However, at low
747 rates of migration between demes ($N_{deme}m$ of 0.1), the DFE was mis-inferred even at 0%
748 selfing, with a bias towards inferring a lower efficacy of selection than the simulated DFE
749 (Figure 7; Supplementary Figure 20). This was largely because the relative increase in
750 intermediate frequency alleles due to population structure as opposed to panmixia
751 (Supplementary Figures 21-22) was falsely inferred as a bottleneck (mean fold change = 0.45-
752 0.50; similar to Chikhi *et al.* 2010) by DFE-alpha, leading to incorrect estimates of the DFE. As
753 expected, these distortions of intermediate frequency alleles in the SFS caused by population
754 structure were observed to increase at higher selfing levels and at lower migration rates, with
755 particularly strong deviations from panmixia observed at $N_{deme}m = 0.1$.
756 Empirical studies that draw from worldwide population samples may knowingly or
757 unknowingly sample unevenly from structured populations when performing DFE inference. To
758 investigate if this has unintended consequences on DFE inference, we repeated our experiments
759 with population structure, altering our sampling strategy to primarily draw genomes from one
760 deme (60%) or two demes (35% from each), with the remaining demes contributing only 10% of
761 the sampled genomes each. As expected, the site frequency spectra from both unevenly sampled
762 populations were observed to be even more distorted at intermediate frequencies than the evenly
763 sampled populations with low migration rates (Supplementary Figures 23-26). For the sampling
764 strategy primarily drawing from one deme, some DFE mis-inference towards nearly neutral and
765 strongly deleterious mutations was observed at 0% and 50% selfing even for $N_{deme}m = 1$ and
766 more strongly at $N_{deme}m = 0.5$, and this effect was stronger at the DFE with predominantly
767 weakly deleterious mutations (Supplementary Figure 27). This effect was also observed for the
768 sampling strategy primarily drawing from two demes, but to a lesser extent (Supplementary
769 Figure 28). At the lowest migration rate, the inferred DFEs for both uneven sampling cases were
770 substantially less deleterious at 0% and 50% selfing than for even sampling, particularly for the
771 DFE with predominantly weakly deleterious mutations (Figure 7). At higher selfing levels, the
772 inferred DFEs for all sampling schemes falsely inferred a larger proportion of weakly deleterious

773 mutations than predicted by the DFE corrected for BGS (Figure 7), likely due to a combination
774 of HRI and uneven sampling. The BGS-corrected DFE was unable to correct for the mis-
775 inference of the DFE for all selfing levels at the lowest migration rate, reflecting the fact that
776 DFE mis-inference is likely driven by changes in the SFS caused by population structure rather
777 than changes in the level of BGS.
778 Overall, these results indicate both DFE inference approaches are fairly robust to
779 population structure in an island model, even with uneven sampling, until the populations
780 become extremely isolated from each other, or individuals are mostly drawn from one deme,
781 especially when the true DFE has a significant proportion of mildly deleterious mutations.
782 Additionally, both low rates of migration and highly uneven sampling result in the inference of
783 an even more weakly deleterious DFE than simulated. Testing DFE inference with more models
784 of population structure and additional sampling strategies might be necessary to interpret
785 empirically estimated DFEs from natural populations.
786
787
788 **DISCUSSION**
789 Inference of the distribution of fitness effects (DFE) of new mutations is a critical step in
790 understanding the forces that shape genetic variation in a population. Population genetic methods
791 to infer the DFE that account for nonequilibrium demography usually assume independent
792 segregation of putatively neutral and selected sites (Eyre-Walker and Keightley 2007; Keightley
793 and Eyre-Walker 2007; Galtier 2016; Tataru *et al.* 2017). However, organisms that have little/ no
794 recombination, for instance, those that undergo high rates of selfing or asexual reproduction, are
795 likely to violate this assumption. A major consequence of strong linkage is the increase in BGS,
796 selective sweeps, and Hill-Robertson effects that lower the efficacy of selection. Particularly in
797 the regime where HRI is pervasive, many linked selected polymorphisms segregate in a
798 population, reducing the population's variance in fitness and thus the efficacy of selection
799 (Comeron and Kreitman 2002; Kaiser and Charlesworth 2009; Seger *et al.* 2010; O'Fallon *et al.*
800 2010; Nicolaisen and Desai 2013). In this study, we demonstrate that when HRI is pervasive, the
801 DFE of new deleterious mutations is mis-inferred. When the regime of classical BGS and sweeps
802 is predominant, population-scaled selection coefficients remain biased (as expected), but
803 accounting for the relative decrease in the rate of coalescence can provide reasonably accurate

804 estimates of the selection coefficients. The latter is applicable to moderately recombining
805 populations/regions. We also find that while purging of partially recessive deleterious mutations
806 does not lead to mis-inference, the presence of cryptic population structure where there is a low
807 rate of migration between subpopulations and/or sampling from predominantly one
808 subpopulation leads to inferring a DFE skewed towards effectively neutral/mildly deleterious
809 class of mutations. Moreover, the proportion of beneficial substitutions (α) is substantially
810 overestimated in highly selfing species, suggesting caution when performing inference in species
811 or genomic regions with little/no recombination.
812
813 **Why is the DFE estimated from *C. elegans* populations not skewed towards mildly**
814 **deleterious mutations?**
815 While our study suggests that DFE inference in highly selfing species should yield DFEs skewed
816 towards weakly/moderately deleterious mutations, surprisingly, the previous empirical estimate
817 of the *C. elegans* DFE using DFE-alpha is heavily skewed towards the class of strongly
818 deleterious mutations ($2N_e\overline{s_d} > 10{,}000$, Gilbert *et al.* 2022). One explanation of this
819 discrepancy is that the mean $2N_e\overline{s_d}$ of the population is even greater than 10,000. Interestingly,
820 direct measurements of fitness-related traits in mutation accumulation lines suggest that *C.*
821 *elegans* has a highly deleterious DFE, with estimates of the mean deleterious selection
822 coefficient ranging from -0.09 to -0.46 (Vassilieva *et al.* 2000; Baer *et al.* 2005; Katju *et al.*
823 2015). Thus, using previously calculated *C. elegans* N_e ranging from 5,000 to 80,000 (Table 4 in
824 Teterina *et al.* 2023), the expected $2NB\overline{s_d}$ would range from 900 to 72,000, consistent with this
825 explanation. However, there are a few major caveats to these observations. (a) The experimental
826 estimates of selection coefficients are likely biased towards more deleterious selection
827 coefficients due to the difficulty of measuring small fitness changes in experimental lines
828 (Davies *et al.* 1999; Eyre-Walker and Keightley 2007), and might not reflect fitness effects in the
829 wild. (b) It is unclear whether previous estimates of the population sizes of *C. elegans*
830 populations using neutral nucleotide diversity (Barrière and Félix 2005; Cutter 2006; Rockman
831 and Kruglyak 2009; Teterina *et al.* 2023) are accurate due to the joint effects of selfing, HRI, and
832 demography (c) Empirical estimates of the deleterious DFE in *C. elegans* (Gilbert *et al.* 2022)
833 were obtained by sampling worldwide rather than from local populations, and thus other factors
834 such as complex demographic history and population structure could play a role as well. For

835 instance, selfing populations are likely to follow extinction-recolonization dynamics
836 (Charlesworth and Wright 2001; Ingvarsson 2002; Wright *et al.* 2013) and such models remain
837 understudied.

838 A second explanation for the discrepancy between the expected and observed DFE in *C.*
839 *elegans* is that the true selfing rate in wild *C. elegans* might be lower than 99%, thus reducing
840 linked effects of selection (Figure 1). Though selfing rate estimates from unique populations
841 range from 80% to ~100% using various methods (Barrière and Félix 2005; Sivasundar and Hey
842 2005; Teterina *et al.* 2023), in general, the strong LD in *C. elegans* populations (haplotype
843 blocks of 2.5 Mb on average; Cutter 2006) along with low frequency of males in wild specimens
844 (Barrière and Félix 2005; Richaud *et al.* 2018) suggest the outcrossing rate is very low in most
845 populations. A recent study using whole-genome sequencing data focusing on Hawaiian *C.*
846 *elegans* estimated a relatively lower selfing rate of 93%, suggesting that selfing rate can vary
847 across populations (Teterina *et al.* 2023). Importantly, as the samples used in Gilbert *et al.*
848 (2022) were unevenly sampled worldwide (with many samples from Hawaiian populations),
849 variation in selfing rate across populations or through time could additionally influence DFE
850 inference results.

851 A third possibility relates to the difficulty in obtaining the SFS using highly inbred
852 strains. The SNP-calling pipeline used to obtain *C. elegans* population-genetic data converted
853 heterozygous sites into homozygous reference or alternate alleles depending on if the mutant was
854 above or below 50% (Cook *et al.* 2017). This method of SNP processing could lead to the
855 inference of a more deleterious DFE if the heterozygote frequency is higher at neutral sites than
856 selected sites by skewing the neutral SFS towards higher frequencies and the selected SFS
857 towards lower frequencies, though the low frequency of heterozygotes in highly selfing
858 populations makes this unlikely to be a large issue. Future studies working with inbred strains
859 should evaluate the effect of employing such SNP processing approaches on population genomic
860 inference.

861 Finally, we have only examined a population under equilibrium in the current study,
862 whereas a recent population expansion/ contraction could decrease the observed effects of
863 interference between selected alleles at multiple loci, allowing for a correct inference of selection
864 coefficients. HRI effects in non-equilibrium populations remain to be studied more thoroughly.
865 Unfortunately, as linked effects of selection will also lead to falsely inferring recent population

866 growth (Supplementary Table 1; Ewing and Jensen 2016; Schrider *et al.* 2016; Johri *et al.* 2021),
867 there is no straightforward solution to accounting for the effects of the true demography (Johri *et*
868 *al.* 2022b). Thus performing a joint inference of demography and the DFE as employed by Johri
869 *et al.* (2020) is likely to be the most promising approach to circumvent this challenge.
870
871 **How broadly do our results apply**?
872 Previous studies (*e.g*., Messer and Petrov 2013; Gilbert *et al.* 2022) that have observed similar
873 biases in inference using DFE-alpha due to linked effects of selection suggested that this might
874 be because DFE-alpha cannot account for the false signal of extreme recent growth generated by
875 hitchhiking effects. Our study shows that DFE mis-inference was similarly observed when using
876 the method GRAPES, which employs a reweighting scheme of the selected relative to the neutral
877 SFS and does not explicitly model a specific demographic history. We, therefore, conclude that
878 the observed mis-inference is a general phenomenon (likely due to a combination of BGS,
879 sweeps, and HRI effects) and not due to errors unique to a particular method like DFE-alpha.
880 Our results have implications for the population genetics of other highly selfing
881 organisms, many of which could fall into a parameter space where linked effects of selection are
882 pervasive. For instance, highly selfing species with large N_e such as *Arabidopsis thaliana*,
883 *Capsella rubella*, *Capsella bursa-pastoris*, and *Capsella orientalis* have all been shown to have
884 more weakly deleterious DFEs than comparable outcrossing species (*A. lyrata* and *C.*
885 *grandiflora;* Douglas *et al.* 2015; Chen *et al.* 2020)*,* consistent with the effects of selection at
886 linked sites potentially playing an important role in determining their genomic diversity. In
887 addition, classical BGS has been predicted to play a more important role in shaping diversity in
888 *C. rubella, A. thaliana*, and *M. truncatula*, than in *C. elegans* populations (Buffalo 2021).
889 A potential limitation of the applicability of our study is that it is not entirely clear what
890 the extent of HRI in natural populations is expected to be. A key factor that determines the extent
891 of HRI is the number (U_d) of new deleterious mutations per genome per generation, with higher
892 values of NU_d relative to NR causing more interference. Thus, the extent of HRI in across
893 species would likely differ due to differences in outcrossing rates, population sizes, mutation and
894 recombination rates, and genome architecture (McVean and Charlesworth 2000; Comeron and
895 Kreitman 2002; Kaiser and Charlesworth 2009; Good *et al.* 2014). For instance, the rate of LD
896 decay is significantly smaller in *C. elegans* where a complete decay of LD occurs over several

897 Mb (Cutter 2006; Rockman and Kruglyak 2009) compared to *A. thaliana* (10-50 kb; Ross-Ibarra
898 *et al.* 2008; Shimizu and Tsuchimatsu 2015), suggesting a higher possibility of HRI affecting
899 DFE inference in *C. elegans*. Interestingly, *C. elegans* has been observed to have a U-shaped
900 SFS in many samples (Freund *et al.* 2023), consistent with HRI, though in empirical data a
901 variety of explanations such as ancestral allele misorientation, positive selection, and various
902 demographic effects could explain a U-shaped SFS (Freund *et al.* 2023). However, some highly
903 selfing species have more coding-dense genomes and are thus predicted to have higher numbers
904 of deleterious point mutations per genome per generation (U_d) relative to *C. elegans* ($U_d =$
905 0.04), which could increase the chances of interference between selected mutations; these
906 include *Oryza sativa* ((99.3% selfing; $\mathrm{U_d} = 0.72$; Lynch *et al.* 2016; Bah *et al.* 2017) and *A.*
907 *thaliana* (97% selfing; $\mathrm{U_d} = 0.29$; Lynch *et al.* 2016). In addition, pathogenic species like
908 *Plasmodium* ($U_d = 0.25$; Lynch *et al.* 2016) that have variable rates of sexual reproduction
909 between genetically identical clones (and thus experience reduced rates of recombination), seem
910 to have nearly identical neutral and selected site frequency spectra (Figure 3 in Parobek *et al.*
911 2016), suggesting that HRI effects might play an important role in shaping variation across their
912 genomes. We therefore also expect DFE inference to be biased due to HRI in asexual organisms,
913 mitochondrial genomes, and the Y chromosome, all of which have low effective recombination
914 rates (Barton and Charlesworth 1998; Weinreich and Rand 2000; Charlesworth and
915 Charlesworth 2000). Importantly, as structural variants are a significant source of deleterious
916 mutations (Adrion *et al.* 2017; Abel *et al.* 2020) accounting for the input of other mutation types,
917 including small insertion-deletions is likely to increase the estimated value of U_d, making HRI
918 more likely in populations with little/no recombination.
919 An interesting exception is the previous study performed in *Eichhornia paniculata*
920 populations (Arunkumar *et al.* 2015), where effects of selection at linked sites did not confound
921 inference of population-scaled selection coefficients. Their simulated populations were
922 comparable to ours – a high selfing rate (98%), a mutation to recombination rate ratio of 0.14 (*vs.*
923 0.11 in this study), a deleterious DFE (with mean $N\overline{s_d} \sim 50 - 100$), and 15,000,000 selected sites
924 (*vs.* 562,500 in this study). However, the expected values of NU_d in the full haploid genomes of
925 *E. paniculata vs. C. elegans* are ~ 25 and ~ 37,125 respectively, assuming 20% and 30% coding
926 density respectively. Higher NU_d will lead to stronger effects of BGS and has been shown to
927 cause populations with moderate selection coefficients that would otherwise be in the classical

928 BGS regime to have pervasive HRI (Good *et al.* 2014), so it is plausible that differences in NU_d
929 explain the differences between our studies.
930
931
932 **Considerations for inferring the DFE in highly selfing organisms**
933 Given our observations, we here provide a few points to consider when inferring the DFE of new
934 mutations in organisms with little/no recombination, where effects of BGS, selective sweeps, or
935 HRI might be pervasive:
936 (1) The DFE of new deleterious mutations estimated using the two-step population-
937 genetic methods is most closely explained by the distribution of $2NBs_d$, which is equivalent to
938 $2N_{emp}(1+F)s_d$ in partially selfing populations. Here N_{emp} represents the effective population
939 size estimated using neutral nucleotide diversity (not accounting for selfing), which includes the
940 effects of BGS and is what is usually estimated using demographic inference approaches that do
941 not account for linked effects of selection. Thus, if there exist accurate experimentally validated
942 estimates of selfing rates, it is possible to accurately infer the distribution of selection
943 coefficients in populations with moderate levels of selfing. However, in many organisms selfing
944 rates are inferred using allele frequencies and those estimates are likely to be biased by
945 population history and effects of selection at linked sites. Moreover, this raises the question of
946 how one can accurately simulate an estimated DFE (in terms of population-scaled selection
947 coefficients) when multiple linked selected sites are to be simulated, which will be especially
948 important to determine the extent of HRI effects in populations with little/no recombination.
949 (2) Different models of population structure and the effects of demographic changes need
950 to be considered to fully understand the robustness of DFE inference. For instance, it is known
951 that local populations of selfing organisms are prone to recurrent extinction and recolonization
952 events (Pannell and Charlesworth 1999; Ingvarsson 2002) which may bias DFE inference
953 further. Indeed, recent field studies of *C. elegans* populations suggest that 3-10 individuals
954 colonize a food source and quickly reproduce to census sizes of up to 10,000 individuals before
955 dispersing in search of new food sources (Barrière and Félix 2005; Richaud *et al.* 2018). When
956 sampling across many demes, we suggest also inferring the DFE in isolated populations in order
957 to minimize biases due to cryptic population structure or uneven sampling and to downsample
958 the number of genomes such that sampling is as even as possible across demes. Sampling

strategies such as a scattered sampling scheme may be useful in removing such bias (Wakeley 1999; Städler *et al.* 2009), though the reduction in sample size may reduce the ability to accurately infer the moderate and deleterious portions of the DFE (Kim *et al.* 2017).

(3) If possible, it could be helpful to infer the DFE in closely related non-selfing species or in different populations of the same species with known differences in selfing rates. For instance, *C. elegans* and *A. thaliana* populations vary in the estimated rates of selfing by ~10%, and the mostly outcrossing *A. lyrata* has several populations that have evolved partial selfing (Mable *et al.* 2005; Bomblies *et al.* 2010; Teterina *et al.* 2023). Though differences such as population structure and demography need to be carefully accounted for, such comparisons across populations/species could also be used to approximate the extent of HRI in a selfing species.

(4) Finally, in the cases where HRI is determined to be extensive, joint inference of demography and the DFE as employed by Johri *et al.* in *D. melanogaster* (2020) and human (2022) populations could be especially useful for DFE inference. They employed an approximate Bayesian computation (Beaumont *et al.* 2002) framework combined with forward simulations to jointly infer parameters of the DFE of new deleterious mutations and an arbitrary size change, while accounting for the effects of selection at linked sites. While highly successful, such an approach has been limited to a relatively simple demographic model of a single size change in one population due to the large number of parameters required to be jointly estimated. In addition, our work here indicates that simulation rescaling may have to be limited to accurately capture the dynamics of Hill-Robertson interference, which will further increase the computational burden of simulations. Thus, if computationally feasible, such an approach could yield the most likely distribution of $2Ns_d$. More importantly, the distribution of $2Ns_d$ describing the fitness effects of new mutations is likely not the distribution of $2Ns_d$ describing the fixation probabilities of new mutations, which will be relatively smaller. Furthermore, the distortions of the SFS from a neutral model caused by interference cannot be explained by any constant N_e (see discussion in Neher 2013; Good *et al.* 2014; Melissa *et al.* 2022). Thus, until theoretical models can accurately estimate the effects of HRI in organisms with little/no recombination with complex DFEs, simulation-based approaches will be the most helpful in inferring the DFE of new mutations in such populations, as well as obtaining the fixation probability of new mutations, which will be altered by HRI.

ACKNOWLEDGEMENTS

We thank Brian Charlesworth for many helpful discussions related to the project and for providing suggestions and comments that improved the manuscript. We are also thankful to Matthew Hartfield for providing helpful comments to improve the manuscript and to Matt Rockman for many helpful discussions and for pointing us to relevant resources available for *C. elegans*. The research in this study was conducted using computational resources provided by ITS Research Computing at the University of North Carolina at Chapel Hill. A.T.D. received support from NIGMS predoctoral training grant 5T32 GM067553. The authors declare no conflicts of interests.

DATA AVAILABILITY

The following data are publicly available on https://github.com/JohriLab/DFESelfing: (1) Data and scripts to reproduce figures; (2) Config files used for DFE inference; (3) Simulation outputs in SLiM format; (4) templates and example scripts for launching SLiM simulations.

REFERENCES

Abel H. J., D. E. Larson, A. A. Regier, C. Chiang, I. Das, *et al.*, 2020 Mapping and characterization of structural variation in 17,795 human genomes. Nature 583: 83–89.

Adrion J. R., M. J. Song, D. R. Schrider, M. W. Hahn, and S. Schaack, 2017 Genome-wide estimates of transposable element insertion and deletion rates in Drosophila melanogaster. Genome biology and evolution 9: 1329–1340.

Agrawal A. F., and M. C. Whitlock, 2011 Inferences about the distribution of dominance drawn from Yeast gene knockout data. Genetics 187: 553–566.

Anderson J. L., L. T. Morran, and P. C. Phillips, 2010 Outcrossing and the maintenance of males within *C. elegans* populations. J. Hered. 101: S62–S74.

Arunkumar R., R. W. Ness, S. I. Wright, and S. C. H. Barrett, 2015 The evolution of selfing is accompanied by reduced efficacy of selection and purging of deleterious mutations. Genetics 199: 817–829.

Baer C. F., F. Shaw, C. Steding, M. Baumgartner, A. Hawkins, *et al.*, 2005 Comparative evolutionary genetics of spontaneous mutations affecting fitness in rhabditid nematodes. Proc. Natl. Acad. Sci. USA 102: 5785–5790.

1025 Bah S., R. van der Merwe, and M. T. Labuschagne, 2017 Estimation of outcrossing rates in
1026 intraspecific (*Oryza sativa*) and interspecific (*Oryza sativa* × *Oryza glaberrima*) rice
1027 under field conditions using agro-morphological markers. Euphytica 213: 81.
1028 Bank C., G. B. Ewing, A. Ferrer-Admettla, M. Foll, and J. D. Jensen, 2014 Thinking too
1029 positive? Revisiting current methods of population genetic selection inference. Trends
1030 Genet. 30: 540–546.
1031 Barrière A., and M.-A. Félix, 2005 High local genetic diversity and low outcrossing rate in
1032 *Caenorhabditis elegans* natural populations. Curr. Biol. 15: 1176–1184.
1033 Barrière A., and M.-A. Félix, 2007 Temporal dynamics and linkage disequilibrium in natural
1034 *Caenorhabditis elegans* populations. Genetics 176: 999–1011.
1035 Barton N. H., and B. Charlesworth, 1998 Why sex and recombination? Science 281: 1986–1990.
1036 Beaumont M. A., W. Zhang, and D. J. Balding, 2002 Approximate Bayesian computation in
1037 population genetics. Genetics 162: 2025–2035.
1038 Becher H., B. C. Jackson, and B. Charlesworth, 2020 Patterns of genetic variability in genomic
1039 regions with low rates of recombination. Curr. Biol. 30: 94-100.e3.
1040 Bomblies K., L. Yant, R. A. Laitinen, S.-T. Kim, J. D. Hollister, *et al.*, 2010 Local-scale patterns
1041 of genetic variability, outcrossing, and spatial structure in natural stands of *Arabidopsis*
1042 *thaliana*. PLoS Genet. 6: e1000890.
1043 Buffalo V., 2021 Quantifying the relationship between genetic diversity and population size
1044 suggests natural selection cannot explain Lewontin's Paradox, (G. Sella, D. Weigel, G.
1045 Sella, and M. Pennell, Eds.). eLife 10: e67509.
1046 *C. elegans* Sequencing Consortium, 1998 Genome sequence of the nematode *C. elegans*: a
1047 platform for investigating biology. Science 282: 2012–8.
1048 Caballero A., P. D. Keightley, and W. G. Hill, 1991 Strategies for increasing fixation
1049 probabilities of recessive mutations. Genet. Res. 58: 129–138.
1050 Caballero A., and W. G. Hill, 1992 Effects of partial inbreeding on fixation rates and variation of
1051 mutant genes. Genetics 131: 493–507.
1052 Campos J. L., and B. Charlesworth, 2019 The effects on neutral variability of recurrent selective
1053 sweeps and background selection. Genetics 212: 287–303.
1054 Charlesworth D., and B. Charlesworth, 1987 Inbreeding depression and its evolutionary
1055 consequences. Annu. Rev. Ecol. Syst. 18: 237–268.
1056 Charlesworth B., 1992 Evolutionary rates in partially self-fertilizing species. Am. Nat. 140: 126–
1057 148.
1058 Charlesworth B., M. T. Morgan, and D. Charlesworth, 1993 The effect of deleterious mutations
1059 on neutral molecular variation. Genetics 134: 1289–1303.
1060 Charlesworth B., 1994 The effect of background selection against deleterious mutations on
1061 weakly selected, linked variants. Genet. Res. 63: 213–227.
1062 Charlesworth B., and D. Charlesworth, 1998 Some evolutionary consequences of deleterious
1063 mutations. Genetica 102: 3–19.
1064 Charlesworth B., and D. Charlesworth, 2000 The degeneration of Y chromosomes. Philos. Trans.
1065 R. Soc. Lond. B. Biol. Sci. 355: 1563–1572.
1066 Charlesworth D., and S. I. Wright, 2001 Breeding systems and genome evolution. Curr. Opin.
1067 Genet. Dev. 11: 685–690.
1068 Charlesworth D., 2003 Effects of inbreeding on the genetic diversity of populations. Philos.
1069 Trans. R. Soc. Lond. B Biol. Sci. 358: 1051–1070.

1070 Charlesworth B., and D. Charlesworth, 2010 *Elements of Evolutionary Genetics*. *Roberts and*
1071 *Company*, *Greenwoord Village, Colorado, USA*.
1072 Charlesworth B., and J. D. Jensen, 2021 Effects of selection at linked sites on patterns of genetic
1073 variability. Annu. Rev. Ecol. Syst. 52: 177–197.
1074 Chen J., S. Glémin, and M. Lascoux, 2020 From drift to draft: How much do beneficial
1075 mutations actually contribute to predictions of Ohta's slightly deleterious model of
1076 molecular evolution? Genetics 214: 1005–1018.
1077 Chikhi L., V. C. Sousa, P. Luisi, B. Goossens, and M. A. Beaumont, 2010 The confounding
1078 effects of population structure, genetic diversity and the sampling scheme on the
1079 detection and quantification of population size changes. Genetics 186: 983–995.
1080 Comeron J. M., M. Kreitman, and M. Aguadé, 1999 Natural selection on synonymous sites is
1081 correlated with gene length and recombination in *Drosophila*. Genetics 151: 239–249.
1082 Comeron J. M., and M. Kreitman, 2002 Population, evolutionary and genomic consequences of
1083 interference selection. Genetics 161: 389–410.
1084 Cook D. E., S. Zdraljevic, J. P. Roberts, and E. C. Andersen, 2017 CeNDR, the *Caenorhabditis*
1085 *elegans* natural diversity resource. Nucleic Acids Res. 45: D650–D657.
1086 Crow J. F., and Kimura, M., 1970 *An Introduction to Population Genetics Theory*. *Harper &*
1087 *Row*, *New York, NY*.
1088 Cutter A. D., 2006 Nucleotide polymorphism and linkage disequilibrium in wild populations of
1089 the partial selfer *Caenorhabditis elegans*. Genetics 172: 171–184.
1090 Cvijović I., B. H. Good, and M. M. Desai, 2018 The effect of strong purifying selection on
1091 genetic diversity. Genetics 209: 1235–1278.
1092 Davies E. K., A. D. Peters, and P. D. Keightley, 1999 High frequency of cryptic deleterious
1093 mutations in *Caenorhabditis elegans*. Science 285: 1748–1751.
1094 Denver D. R., K. Morris, M. Lynch, and W. K. Thomas, 2004 High mutation rate and
1095 predominance of insertions in the *Caenorhabditis elegans* nuclear genome. Nature 430:
1096 679–682.
1097 Douglas G. M., G. Gos, K. A. Steige, A. Salcedo, K. Holm, *et al.*, 2015 Hybrid origins and the
1098 earliest stages of diploidization in the highly successful recent polyploid *Capsella bursa-*
1099 *pastoris*. Proc. Natl. Acad. Sci. USA 112: 2806–2811.
1100 Estes S., P. C. Phillips, D. R. Denver, W. K. Thomas, and M. Lynch, 2004 Mutation
1101 accumulation in populations of varying size: The distribution of mutational effects for
1102 fitness correlates in *Caenorhabditis elegans*. Genetics 166: 1269–1279.
1103 Ewens W. J., 1979 *Mathematical Population Genetics*. *Springer*, *Berlin*.
1104 Ewing G. B., and J. D. Jensen, 2016 The consequences of not accounting for background
1105 selection in demographic inference. Mol. Ecol. 25: 135–141.
1106 Eyre-Walker A., M. Woolfit, and T. Phelps, 2006 The distribution of fitness effects of new
1107 deleterious amino acid mutations in humans. Genetics 173: 891–900.
1108 Eyre-Walker A., and P. D. Keightley, 2007 The distribution of fitness effects of new mutations.
1109 Nat. Rev. Genet. 8: 610–618.
1110 Eyre-Walker A., and P. D. Keightley, 2009 Estimating the rate of adaptive molecular evolution
1111 in the presence of slightly deleterious mutations and population size change. Mol. Biol.
1112 Evol. 26: 2097–2108.
1113 Felsenstein J., 1974 The evolutionary advantage of recombination. Genetics 78: 737–756.

1114 Freund F., E. Kerdoncuff, S. Matuszewski, M. Lapierre, M. Hildebrandt, *et al.*, 2023 Interpreting
1115 the pervasive observation of U-shaped Site Frequency Spectra. PLoS Genet. 19:
1116 e1010677.
1117 Galtier N., 2016 Adaptive protein evolution in animals and the effective population size
1118 hypothesis. PLoS Genet. 12: e1005774.
1119 Garcia J. A., and K. E. Lohmueller, 2021 Negative linkage disequilibrium between amino acid
1120 changing variants reveals interference among deleterious mutations in the human
1121 genome. PLoS Genet. 17: e1009676.
1122 Gilbert K. J., S. Zdraljevic, D. E. Cook, A. D. Cutter, E. C. Andersen, *et al.*, 2022 The
1123 distribution of mutational effects on fitness in *Caenorhabditis elegans* inferred from
1124 standing genetic variation, (L. Moyle, Ed.). Genetics 220: iyab166.
1125 Glémin S., 2003 How are deleterious mutations purged? Drift versus nonrandom mating.
1126 Evolution 57: 2678–2687.
1127 Good B. H., A. M. Walczak, R. A. Neher, and M. M. Desai, 2014 Genetic diversity in the
1128 interference selection limit. PLoS Genet. 10: e1004222.
1129 Goodwillie C., S. Kalisz, and C. G. Eckert, 2005 The evolutionary enigma of mixed mating
1130 systems in plants: Occurrence, theoretical explanations, and empirical evidence. Annu.
1131 Rev. Ecol. Syst. 36: 47–79.
1132 Haller B. C., and P. W. Messer, 2023 SLiM 4: Multispecies eco-evolutionary modeling. Am.
1133 Nat. 201: E127–E139.
1134 Hartfield M., and S. Glémin, 2014 Hitchhiking of deleterious alleles and the cost of adaptation in
1135 partially selfing species. Genetics 196: 281–293.
1136 Hartfield M., and S. Glémin, 2016 Limits to adaptation in partially selfing species. Genetics 203:
1137 959–974.
1138 Hartfield M., and T. Bataillon, 2020 Selective sweeps under dominance and inbreeding. G3 10:
1139 1063–1075.
1140 Hedrick P. W., 1980 Hitchhiking: a comparison of linkage and partial selfing. Genetics 94: 791–
1141 808.
1142 Hill W. G., and A. Robertson, 1966 The effect of linkage on limits to artificial selection. Genet.
1143 Res. 8: 269–294.
1144 Hodgkin J., 1983 Male phenotypes and mating efficiency in *Caenorhabditis elegans*. Genetics
1145 103: 43–64.
1146 Huang X., A. L. Fortier, A. J. Coffman, T. J. Struck, M. N. Irby, *et al.*, 2021 Inferring genome-
1147 wide correlations of mutation fitness effects between populations. Mol. Biol. Evol. 38:
1148 4588–4602.
1149 Huber C. D., B. Y. Kim, C. D. Marsden, and K. E. Lohmueller, 2017 Determining the factors
1150 driving selective effects of new nonsynonymous mutations. Proc. Natl. Acad. Sci. USA
1151 114: 4465–4470.
1152 Ingvarsson P. K., 2002 A metapopulation perspective on genetic diversity and differentiation in
1153 partially self-fertilizing plants. Evolution 56: 2368–2373.
1154 Jarne P., and J. R. Auld, 2006 Animals mix it up too: the distribution of self-fertilization among
1155 hermaphroditic animals. Evolution 60: 1816–1824.
1156 Johri P., B. Charlesworth, and J. D. Jensen, 2020 Toward an evolutionarily appropriate null
1157 model: jointly inferring demography and purifying selection. Genetics 215: 173–192.

1158 Johri P., K. Riall, H. Becher, L. Excoffier, B. Charlesworth, *et al.*, 2021 The impact of purifying
1159 and background selection on the inference of population history: problems and prospects.
1160 Mol. Biol. Evol. 38: 2986–3003.
1161 Johri P., C. F. Aquadro, M. Beaumont, B. Charlesworth, L. Excoffier, *et al.*, 2022a
1162 Recommendations for improving statistical inference in population genomics. PLoS Biol.
1163 20: e3001669.
1164 Johri P., A. Eyre-Walker, R. N. Gutenkunst, K. E. Lohmueller, and J. D. Jensen, 2022b On the
1165 prospect of achieving accurate joint estimation of selection with population history.
1166 Genome Biol. Evol. 14: evac088.
1167 Kaiser V. B., and B. Charlesworth, 2009 The effects of deleterious mutations on evolution in
1168 non-recombining genomes. Trends Genet. 25: 9–12.
1169 Kamran-Disfani A., and A. F. Agrawal, 2014 Selfing, adaptation and background selection in
1170 finite populations. J. Evol. Biol. 27: 1360–1371.
1171 Katju V., L. B. Packard, L. Bu, P. D. Keightley, and U. Bergthorsson, 2015 Fitness decline in
1172 spontaneous mutation accumulation lines of *Caenorhabditis elegans* with varying
1173 effective population sizes. Evolution 69: 104–16.
1174 Keightley P. D., and A. Eyre-Walker, 2007 Joint inference of the distribution of fitness effects of
1175 deleterious mutations and population demography based on nucleotide polymorphism
1176 frequencies. Genetics 177: 2251–2261.
1177 Kim B. Y., C. D. Huber, and K. E. Lohmueller, 2017 Inference of the distribution of selection
1178 coefficients for new nonsynonymous mutations using large samples. Genetics 206: 345–
1179 361.
1180 Konrad A., M. J. Brady, U. Bergthorsson, and V. Katju, 2019 Mutational landscape of
1181 spontaneous base substitutions and small indels in experimental *Caenorhabditis elegans*
1182 populations of differing size. Genetics 212: 837–854.
1183 Kousathanas A., and P. D. Keightley, 2013 A comparison of models to infer the distribution of
1184 fitness effects of new mutations. Genetics 193: 1197–1208.
1185 Lewontin R. C., 1964 The interaction of selection and linkage. I. general considerations;
1186 heterotic models. Genetics 49: 49–67.
1187 Lewontin R. C., 1988 On measures of gametic disequilibrium. Genetics 120: 849–852.
1188 Li W.-H., 1987 Models of nearly neutral mutations with particular implications for nonrandom
1189 usage of synonymous codons. J. Mol. Evol. 24: 337–345.
1190 Lipinski K. J., J. C. Farslow, K. A. Fitzpatrick, M. Lynch, V. Katju, *et al.*, 2011 High
1191 spontaneous rate of gene duplication in Caenorhabditis elegans. Current Biology 21:
1192 306–310.
1193 Lynch M., M. S. Ackerman, J.-F. Gout, H. Long, W. Sung, *et al.*, 2016 Genetic drift, selection
1194 and the evolution of the mutation rate. Nat. Rev. Genet. 17: 704–714.
1195 Mable B. K., A. V. Robertson, S. Dart, C. Di Berardo, and L. Witham, 2005 Breakdown of self-
1196 incompatibility in the perennial *Arabidopsis lyrata* (*Brassicaceae*) and its genetic
1197 consequences. Evolution 59: 1437–1448.
1198 Manna F., G. Martin, and T. Lenormand, 2011 Fitness landscapes: An alternative theory for the
1199 dominance of mutation. Genetics 189: 923–937.
1200 Maruyama T., 1970 Effective number of alleles in a subdivided population. Theor. Popul. Biol.
1201 1: 273–306.

McVean G. A., and B. Charlesworth, 2000 The effects of Hill-Robertson interference between weakly selected mutations on patterns of molecular evolution and variation. Genetics 155: 929–944.

Melissa M. J., B. H. Good, D. S. Fisher, and M. M. Desai, 2022 Population genetics of polymorphism and divergence in rapidly evolving populations. Genetics 221: iyac053.

Messer P. W., and D. A. Petrov, 2013 Frequent adaptation and the McDonald-Kreitman test. Proc. Natl. Acad. Sci. USA 110: 8615–8620.

Neher R. A., 2013 Genetic draft, selective interference, and population genetics of rapid adaptation. Annu. Rev. Ecol. Syst. 44: 195–215.

Neher R. A., and O. Hallatschek, 2013 Genealogies of rapidly adapting populations. Proc. Natl. Acad. Sci. USA 110: 437–442.

Nei M., 1968 The frequency distribution of lethal chromosomes in finite populations. Proc. Natl. Acad. Sci. USA 60: 517–524.

Nei M., 1973 Analysis of gene diversity in subdivided populations. Proc. Natl. Acad. Sci. USA 70: 3321–3323.

Nei M., and F. Tajima, 1981 DNA polymorphism detectable by restriction endonucleases. Genetics 97: 145–163.

Nicolaisen L. E., and M. M. Desai, 2013 Distortions in genealogies due to purifying selection and recombination. Genetics 195: 221–230.

Nordborg M., 2000 Linkage disequilibrium, gene trees and selfing: an ancestral recombination graph with partial self-fertilization. Genetics 154: 923–929.

O'Fallon B. D., J. Seger, and F. R. Adler, 2010 A continuous-state coalescent and the impact of weak selection on the structure of gene genealogies. Mol. Biol. Evol. 27: 1162–1172.

Pannell J. R., and B. Charlesworth, 1999 Neutral genetic diversity in a metapopulation with recurrent local extinction and recolonization. Evolution 53: 664–676.

Parobek C. M., J. T. Lin, D. L. Saunders, E. J. Barnett, C. Lon, *et al.*, 2016 Selective sweep suggests transcriptional regulation may underlie *Plasmodium vivax* resilience to malaria control measures in Cambodia. Proc. Natl. Acad. Sci. USA 113: E8096–E8105.

Pollak E., 1987 On the theory of partially inbreeding finite populations. I. Partial selfing. Genetics 117: 353–360.

Richaud A., G. Zhang, D. Lee, J. Lee, and M.-A. Félix, 2018 The Local Coexistence Pattern of Selfing Genotypes in Caenorhabditis elegans Natural Metapopulations. Genetics 208: 807–821.

Rockman M. V., and L. Kruglyak, 2009 Recombinational landscape and population genomics of *Caenorhabditis elegans*. PLoS Genet. 5: e1000419.

Ross-Ibarra J., S. I. Wright, J. P. Foxe, A. Kawabe, L. DeRose-Wilson, *et al.*, 2008 Patterns of polymorphism and demographic history in natural populations of *Arabidopsis lyrata*. PLoS One 3: e2411.

Roze D., and T. Lenormand, 2005 Self-fertilization and the evolution of recombination. Genetics 170: 841–857.

Sanjuán R., A. Moya, and S. F. Elena, 2004 The distribution of fitness effects caused by single-nucleotide substitutions in an RNA virus. Proc. Natl. Acad. Sci. USA 101: 8396–8401.

Saxena A. S., M. P. Salomon, C. Matsuba, S.-D. Yeh, and C. F. Baer, 2019 Evolution of the mutational process under relaxed selection in *Caenorhabditis elegans*. Mol. Biol. Evol. 36: 239–251.

Schrider D. R., A. G. Shanku, and A. D. Kern, 2016 Effects of linked selective sweeps on demographic inference and model selection. Genetics 204: 1207–1223.
Seger J., W. A. Smith, J. J. Perry, J. Hunn, Z. A. Kaliszewska, *et al.*, 2010 Gene genealogies strongly distorted by weakly interfering mutations in constant environments. Genetics 184: 529–545.
Shimizu K. K., and T. Tsuchimatsu, 2015 Evolution of selfing: recurrent patterns in molecular adaptation. Annu. Rev. Ecol. Syst. 46: 593–622.
Sicard A., and M. Lenhard, 2011 The selfing syndrome: a model for studying the genetic and evolutionary basis of morphological adaptation in plants. Ann. Bot. 107: 1433–1443.
Simmons M. J., and J. F. Crow, 1977 Mutations affecting fitness in *Drosophila* populations. Ann. Rev. Genet. 11: 49–78.
Sivasundar A., and J. Hey, 2005 Sampling from natural populations with RNAI reveals high outcrossing and population structure in Caenorhabditis elegans. Curr. Biol. 15: 1598–1602.
Slatkin M., and L. Voelm, 1991 F_{ST} in a hierarchical island model. Genetics 127: 627–629.
Städler T., B. Haubold, C. Merino, W. Stephan, and P. Pfaffelhuber, 2009 The impact of sampling schemes on the site frequency spectrum in nonequilibrium subdivided populations. Genetics 182: 205–216.
Tataru P., M. Mollion, S. Glémin, and T. Bataillon, 2017 Inference of distribution of fitness effects and proportion of adaptive substitutions from polymorphism data. Genetics 207: 1103–1119.
Teterina A. A., J. H. Willis, M. Lukac, R. Jovelin, A. D. Cutter, *et al.*, 2023 Genomic diversity landscapes in outcrossing and selfing *Caenorhabditis* nematodes. PLoS Genet. 19: e1010879.
Thornton K., 2003 libsequence: a C++ class library for evolutionary genetic analysis. Bioinformatics 19: 2325–2327.
Vassilieva L. L., A. M. Hook, and M. Lynch, 2000 The fitness effects of spontaneous mutations in *Caenorhabditis elegans*. Evolution 54: 1234–1246.
Wade E. E., C. C. Kyriazis, M. I. A. Cavassim, and K. E. Lohmueller, 2023 Quantifying the fraction of new mutations that are recessive lethal. Evolution 77: 1539–1549.
Wakeley J., 1999 Nonequilibrium migration in human history. Genetics 153: 1863–1871.
Walczak A. M., L. E. Nicolaisen, J. B. Plotkin, and M. M. Desai, 2012 The structure of genealogies in the presence of purifying selection: a fitness-class coalescent. Genetics 190: 753–779.
Watterson G. A., 1975 On the number of segregating sites in genetical models without recombination. Theor. Popul. Biol. 7: 256–276.
Weinreich D. M., and D. M. Rand, 2000 Contrasting patterns of nonneutral evolution in proteins encoded in nuclear and mitochondrial genomes. Genetics 156: 385–399.
Williamson S. H., R. Hernandez, A. Fledel-Alon, L. Zhu, R. Nielsen, *et al.*, 2005 Simultaneous inference of selection and population growth from patterns of variation in the human genome. Proc. Natl. Acad. Sci. USA 102: 7882–7887.
Wloch D. M., K. Szafraniec, R. H. Borts, and R. Korona, 2001 Direct estimate of the mutation rate and the distribution of fitness effects in the yeast *Saccharomyces cerevisiae*. Genetics 159: 441–452.
Wright S. I., S. Kalisz, and T. Slotte, 2013 Evolutionary consequences of self-fertilization in plants. Proc. R. Soc. Lond. B 280: 20130133.

Zeng K., and B. Charlesworth, 2011 The joint effects of background selection and genetic recombination on local gene genealogies. Genetics 189: 251–266.
Zeng K., and P. Corcoran, 2015 The effects of background and interference selection on patterns of genetic variation in subdivided populations. Genetics 201: 1539–1554.

FIGURES AND TABLES

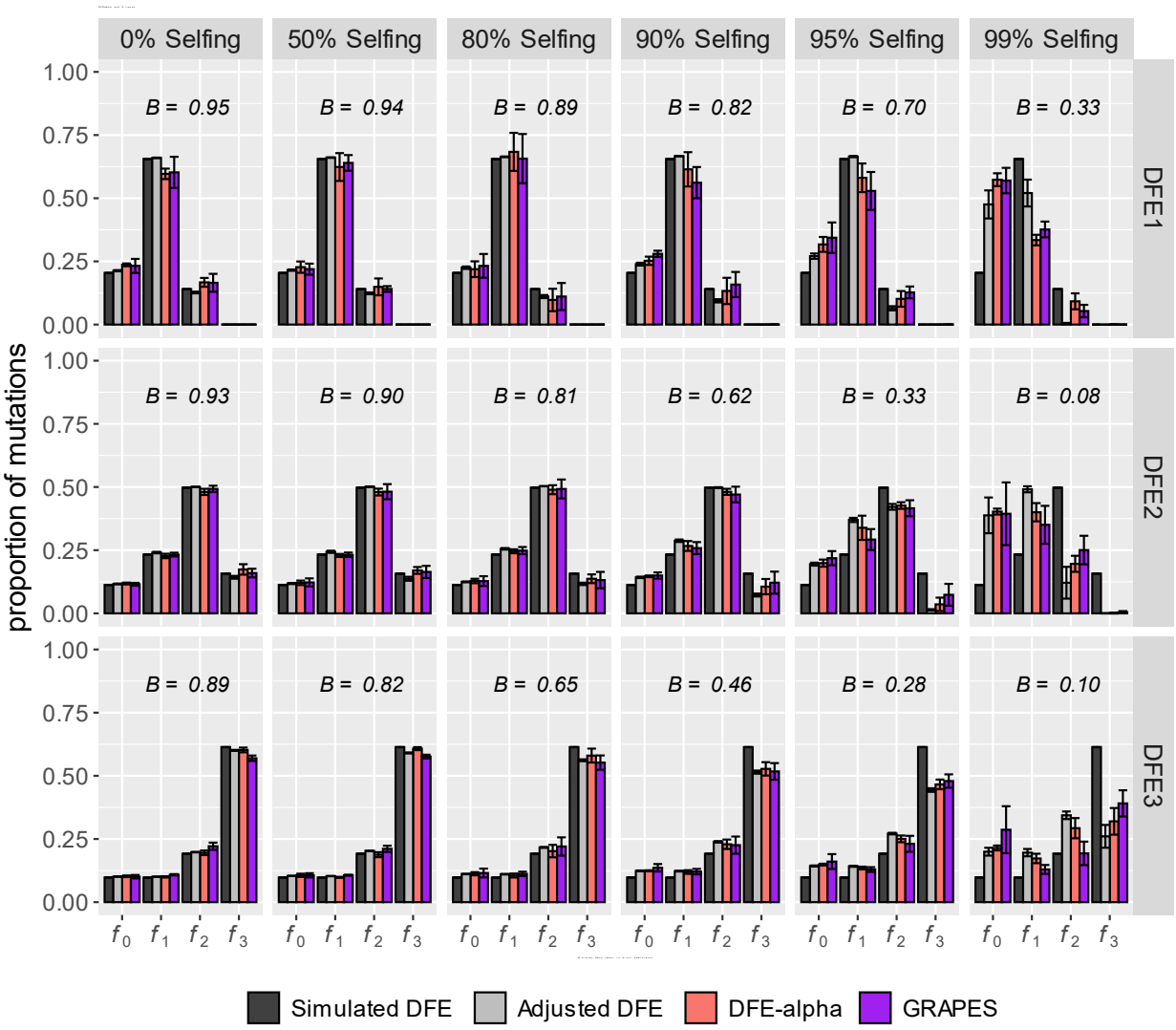

Figure 1: Effects of selfing on the inference of the DFE of new deleterious mutations using DFE-alpha (red bars) and GRAPES (purple bars). Results are shown in terms of the proportion of mutations in effectively neutral (f_0), weakly deleterious (f_1), moderately deleterious (f_2) and strongly deleterious (f_3) classes. Selfing rates were varied between 0 and 99 %. The nucleotide site diversity with background selection (B) relative to its expectation under strict neutrality is shown in each panel. The simulated (black bars) and adjusted (grey bars) DFE represents the distribution of $2Ns_d$ and $2NBs_d$ respectively. The error bars denote the standard deviation of proportions estimated from 5 independent replicates.

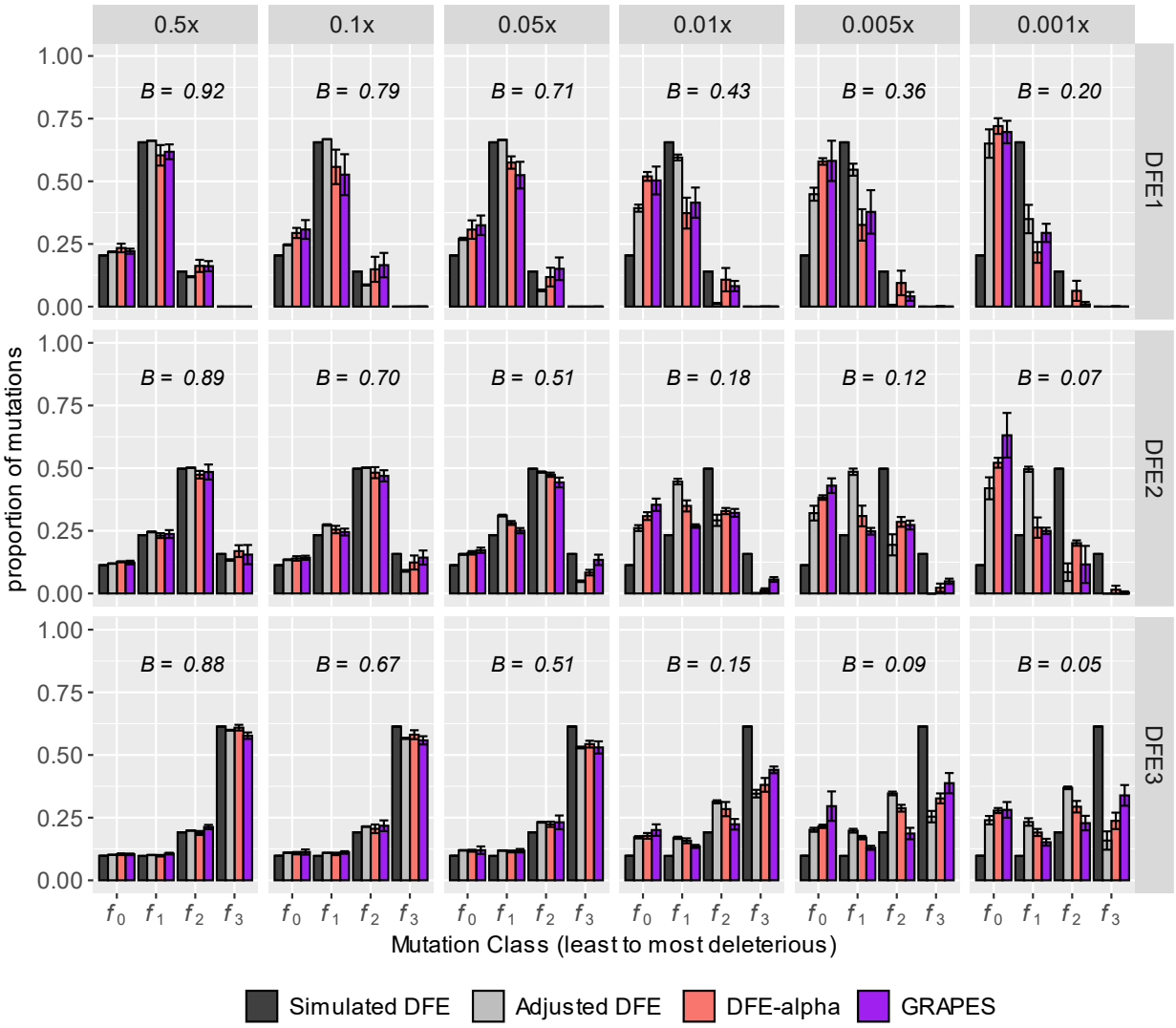

Figure 2: Effects of low recombination rate on the inference of the DFE of new deleterious mutations using DFE-alpha (red bars) and GRAPES (purple bars). Results are shown in terms of the proportion of mutations in effectively neutral (f_0), weakly deleterious (f_1), moderately deleterious (f_2) and strongly deleterious (f_3) classes. Recombination rates were varied between $0.5 \times$ mean and $0.001 \times$ mean, where the mean recombination rate was 3.12×10^{-8} per site/generations. The nucleotide site diversity with background selection (B) relative to its expectation under strict neutrality is shown in each panel. The simulated DFE (shown in black) and adjusted DFE (shown in grey) represents the distribution of $2Ns_d$ and $2NBs_d$ respectively. The error bars denote the standard deviation of proportions estimated from 5 independent replicates.

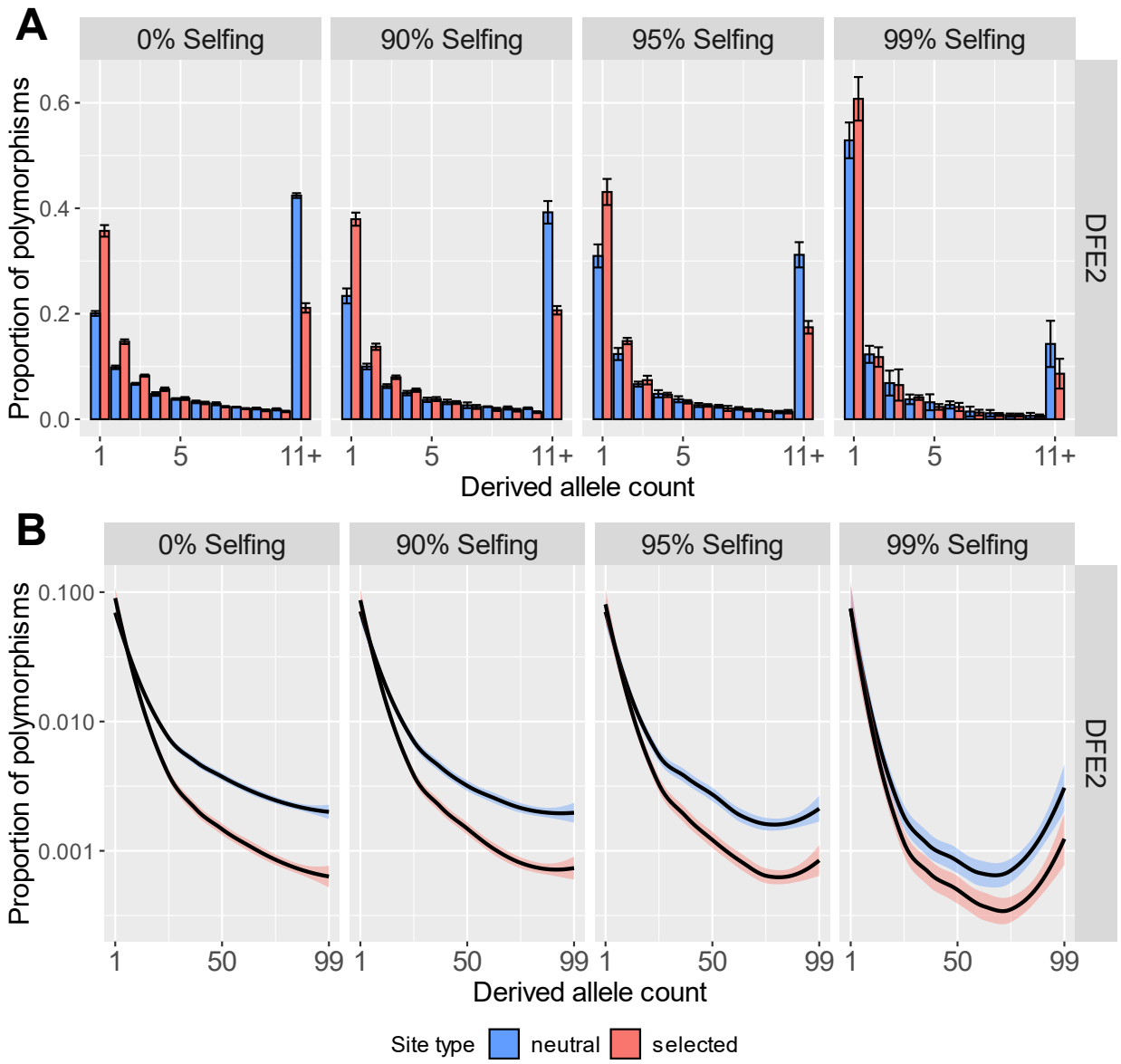

Figure 3: Site frequency spectra of neutral and selected alleles from 100 genomes sampled from simulations where all selected mutations were deleterious, for the moderately deleterious DFE (DFE2). For **(A)** the y-axis represents the proportion of segregating polymorphisms that fall into the given derived allele count. The last class (11+) refers to the derived allele counts 11-99. The error bars denote the standard deviation of proportions estimated from 5 independent replicates. For **(B)** the y-axis is plotted on a log scale, with all derived allele counts displayed. Lines were smoothed with LOESS.

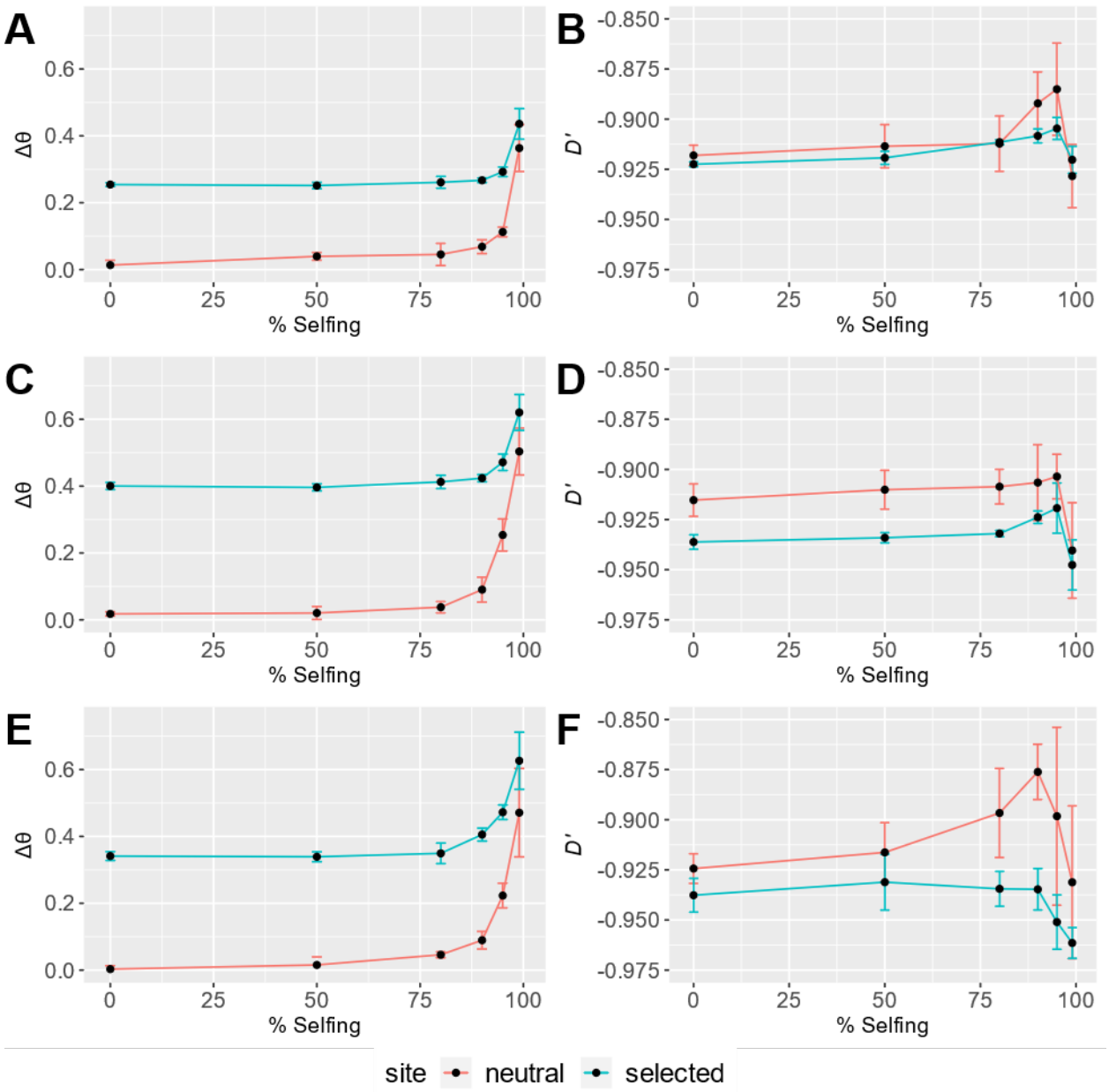

Figure 4: Effects of selfing on the SFS and linkage disequilibrium (LD) at neutral (red lines) and selected (blue lines) sites. The skew in the SFS was quantified using $\Delta\theta$ for DFE1 (**A**), DFE2 (**C**), and DFE3 (**E**), calculated using alleles at all frequencies, while LD was summarized by the statistic D' for DFE1 (**B**), DFE2 (**D**), and DFE3 (**F**), calculated for alleles at frequencies of 1%-5%. The error bars denote the standard deviation of the genome-wide average of each summary statistic estimated from 5 independent replicates.

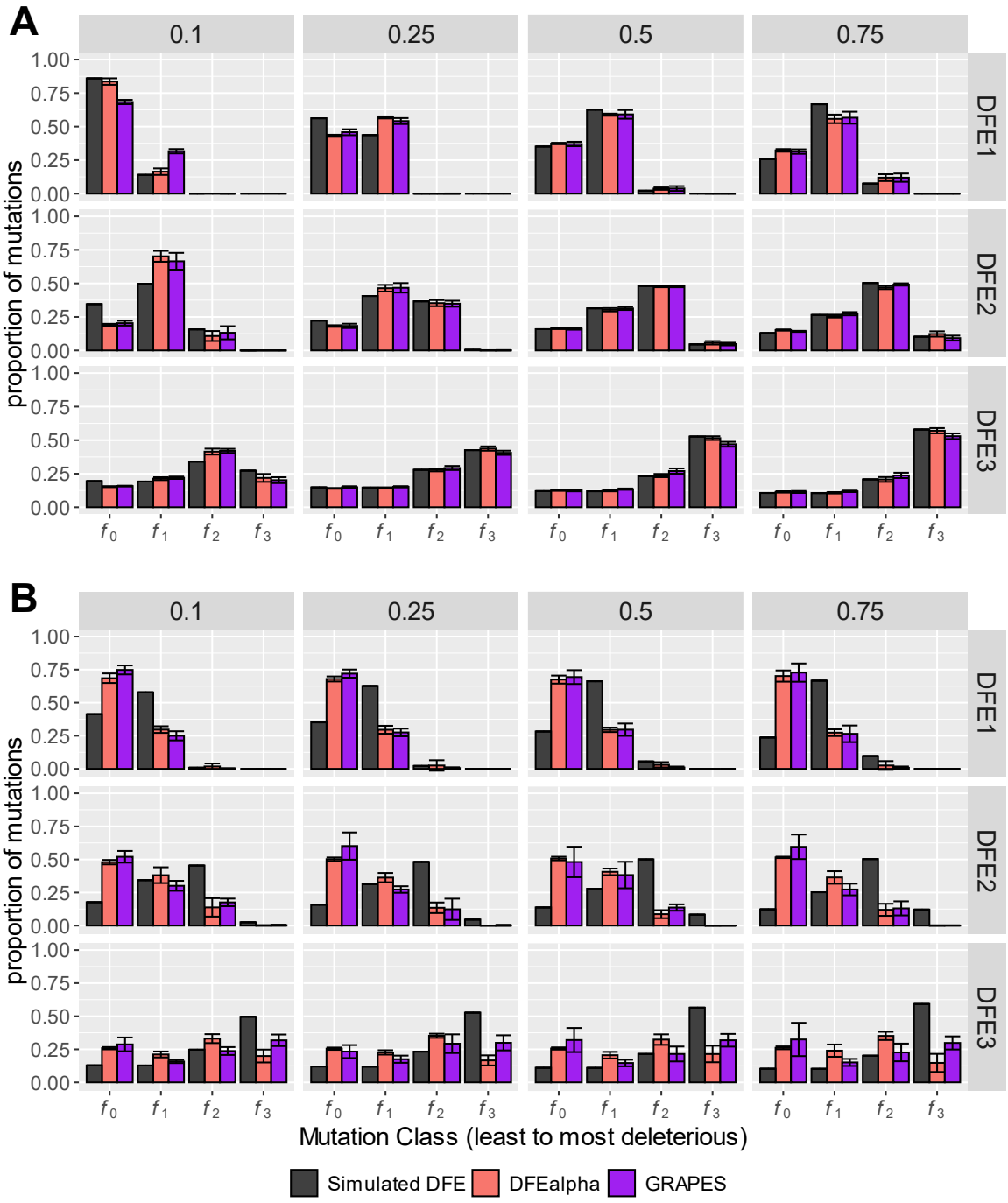

Figure 5: Effects of selfing on DFE inference of new deleterious mutations with varying dominance coefficients using DFE-alpha (red bars) and GRAPES (purple bars). The dominance of selected mutations is noted at the top of each column. Results are shown for populations with **(A)** 0% selfing and **(B)** 99% selfing. Here the effectively neutral (f_0), weakly deleterious (f_1), moderately deleterious (f_2) and strongly deleterious (f_3) classes represent $0 < 2N_{self}s_d h_{self} < 1$, $1 < 2N_{self}s_d h_{self} < 10$, $10 < 2N_{self}s_d h_{self} < 100$, and $100 < 2N_{self}s_d h_{self} < 2N_{self}$, respectively. The error bars denote the standard deviation of proportions estimated from 5 independent replicates.

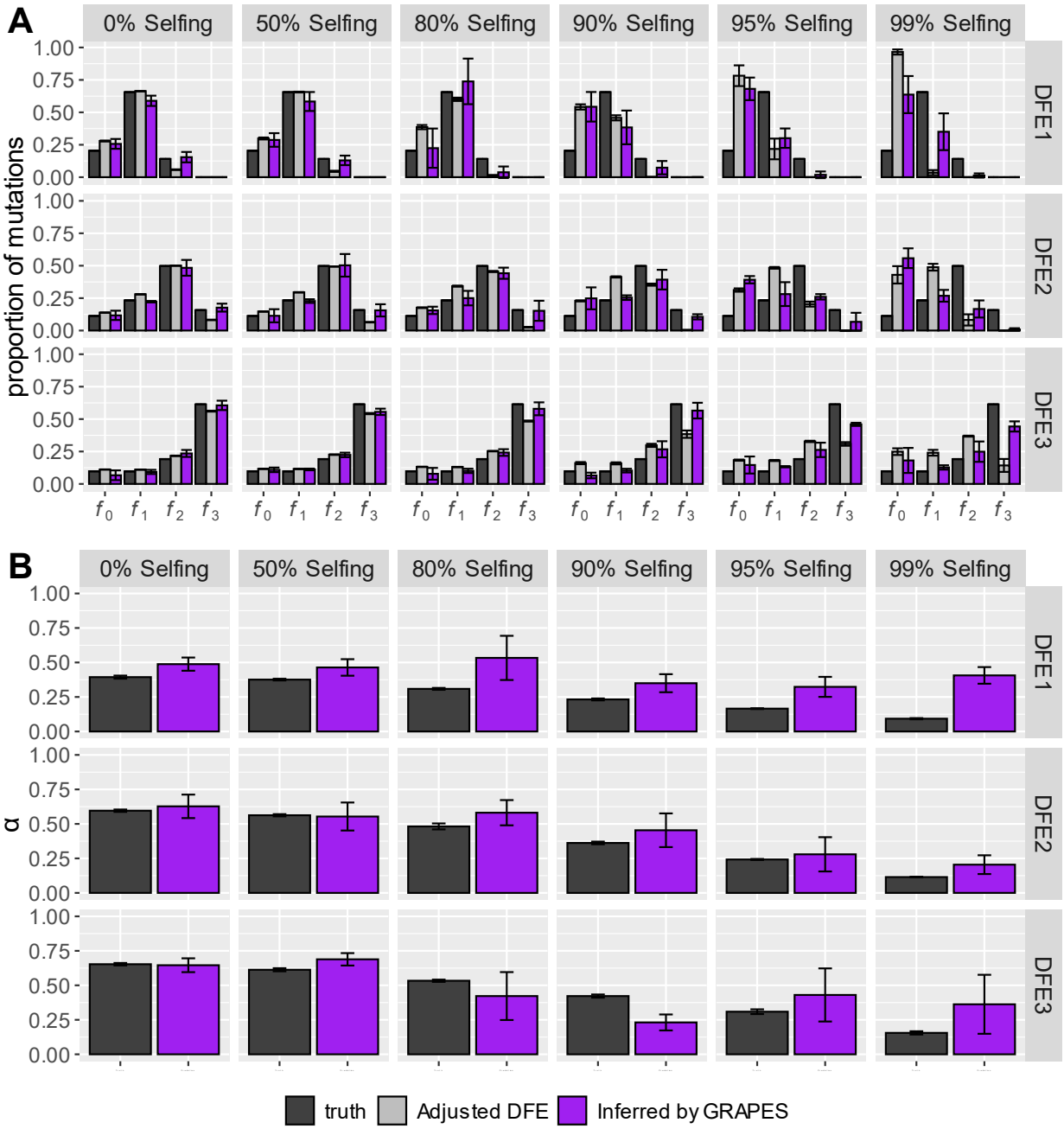

Figure 6. Effects of selfing on the inference of (A) the DFE of new deleterious mutations and (B) the proportion of beneficial fixations (α) using GRAPES (shown in purple bars). (A) Results are shown in terms of the proportion of mutations in effectively neutral (f_0), weakly deleterious (f_1), moderately deleterious (f_2) and strongly deleterious (f_3) classes. The adjusted DFE represents the distribution of $2N(\pi_{obs}/\pi_{exp})s_d$, where π_{obs} is the neutral nucleotide site diversity observed in each scenario and π_{exp} is the neutral nucleotide site diversity expected in a population of size N at strict neutrality. For both (A) and (B), 0.1% of new exonic mutations were beneficial and exponentially distributed with a mean $2Ns_a = 200$. The error bars denote the standard deviation of proportions estimated from 5 independent replicates.

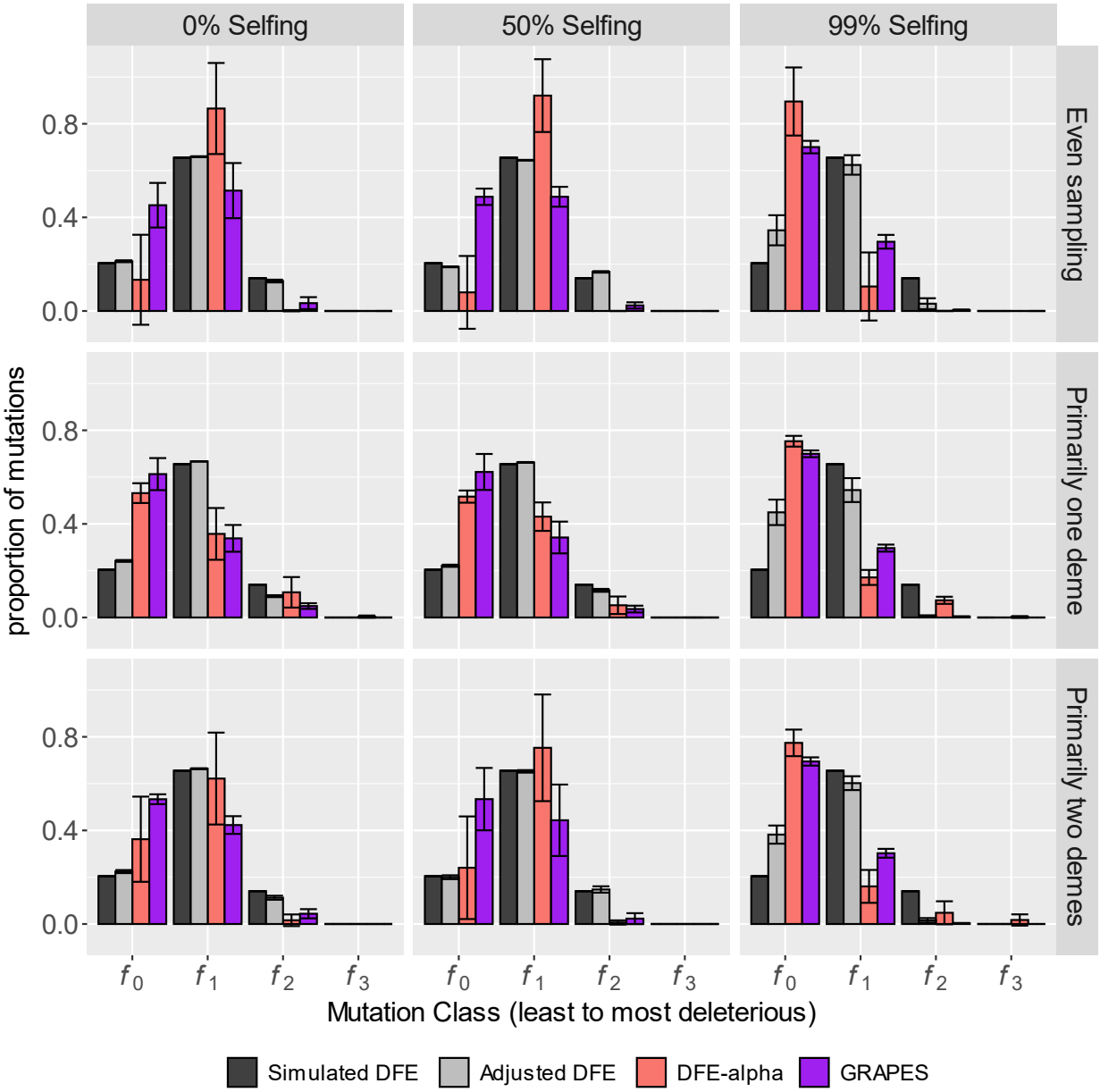

Figure 7 Effects of uneven sampling, population structure, and selfing on the inference of the DFE of new deleterious mutations using DFE-alpha (red bars) and GRAPES (purple bars). Results are shown in terms of the proportion of mutations in effectively neutral (f_0), weakly deleterious (f_1), moderately deleterious (f_2) and strongly deleterious (f_3) classes. Populations were simulated under an island model with five demes such that the metapopulation effective size was equal to 5000 at 0% selfing and $N_{deme}m$ was 0.1. Results are shown for the most weakly deleterious DFE (*i.e.*, DFE1). The error bars denote the standard deviation of proportions estimated from 5 independent replicates. Rows represent the sampling scheme for genomes, where sampling was even, sampling was primarily from one deme, or sampling was primarily from two demes.

Table 1: Parameters of the simulated DFEs of deleterious mutations in terms of the proportion of mutations in effectively neutral (f_0), weakly deleterious (f_1), moderately deleterious (f_2) and strongly deleterious (f_3) classes. DFEs consisted of predominantly mildly deleterious (DFE1), moderately deleterious (DFE2), or strongly deleterious (DFE3) mutations.

	β	$2Ns_d$	f_0	f_1	f_2	f_3
DFE1	0.9	5	0.204	0.655	0.140	0.000
DFE2	0.5	50	0.113	0.233	0.497	0.157
DFE3	0.3	1000	0.098	0.097	0.192	0.614